Half-explicit timestepping schemes on velocity level based on time-discontinuous Galerkin methods

Thorsten Schindler, Shahed Rezaei, Jochen Kursawe, Vincent Acary

Texte

Half-explicit timestepping schemes on velocity level based on time-discontinuous Galerkin methods

Thorsten Schindler, Shahed Rezaei, Jochen Kursawe, Vincent Acary

RESEARCH REPORT
N° 8623
October 2014
Project-Team Bipop

ISSN 0249-6399 ISRN INRIA/RR--8623--FR+ENG

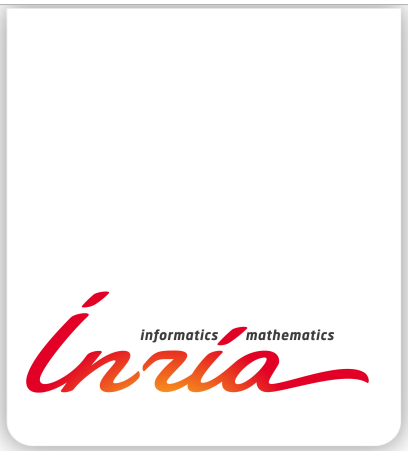

Half-explicit timestepping schemes on velocity level based on time-discontinuous Galerkin methods

Thorsten Schindler*, Shahed Rezaei †, Jochen Kursawe ‡, Vincent Acary§

Project-Team Bipop

Research Report n° 8623 — October 2014 — 44 pages

email : thorsten.schindler@mytum.de, shahed.rezaei@rwth-aachen.de, Jochen.Kursawe@maths.ox.ac.uk, vincent.acary@inria.fr

* Technische Universität München,Institute of Applied Mechanics, Boltzmannstraße 15, 85748 Garching, Germany
† RWTH Aachen, Institute of Applied Mechanics, Mies-van-der-Rohe-Str. 1, 52074 Aachen, Germany
‡ Mathematical Institute, University of Oxford, Andrew Wiles Building, Radcliffe Observatory Quarter, Woodstock Road, Oxford OX2 6GG, United Kingdom
§ INRIA Rhône-Alpes, Centre de recherche Grenoble, 655 avenue de l'Europe, Inovallée de Montbonnot, 38334 St Ismier Cedex, France

RESEARCH CENTRE
GRENOBLE – RHÔNE-ALPES

Inovallée
655 avenue de l'Europe Montbonnot
38334 Saint Ismier Cedex

Abstract: This paper presents a time-discretization scheme for the simulation of nonsmooth mechanical systems. These consist of rigid and flexible bodies, joints as well as contacts and impacts with dry friction. The benefit of the proposed formalism is both the consistent treatment of velocity jumps, e.g. due to impacts, and the automatic local order elevation in non-impulsive intervals at the same time. For an appropriate treatment of constraints in impulsive and non-impulsive intervals, constraints are implicitly formulated on velocity level in terms of an augmented Lagrangian technique [5]. They are satisfied exactly without any penetration. For efficiency reasons, all other evaluations are explicit which yields a half-explicit method [9, 10, 43, 44, 7, 29, 30].
The numerical scheme is an extended timestepping scheme for nonsmooth dynamics according to Moreau [42]. It is based on time-discontinuous Galerkin methods to carry over higher order trial functions of event-driven integration schemes to consistent timestepping schemes for nonsmooth dynamical systems with friction and impacts. Splitting separates the portion of impulsive contact forces from the portion of non-impulsive contact forces. Impacts are included within the discontinuity of the piecewise continuous trial functions, i.e., with first-order accuracy. Non-impulsive contact forces are integrated with respect to the local order of the trial functions. In order to satisfy the constraints, a set of nonsmooth equations has to be solved in each time step depending on the number of stages; the solution of the velocity jump together with the corresponding impulse yields another nonsmooth equation. All nonsmooth equations are treated separately by semi-smooth Newton methods.
The integration scheme on acceleration level was first introduced in [51] labeled "forecasting trapezoidal rule". It was analyzed and applied to a decoupled bouncing ball example concerning principal suitability without taking friction into account. In this work, the approach is algorithmically specified, improved and applied to nonlinear multi-contact examples with friction. It is compared to other numerical schemes and it is shown that the newly proposed integration scheme yields a unified behavior for the description of contact mechanical problems.

Key-words: timestepping scheme, discontinuous Galerkin method, nonsmooth dynamics, flexible multi-body system, friction, impact, index reduction

Schémas d'intégration en temps semi–explicites au niveau des vitesses basés sur des méthodes de Galerkin discontinues en temps.

Résumé : Cet article présente un schéma d'intégration en temps pour la simulations des systèmes mécaniques non–réguliers. Ces systèmes sont constitués de cops flexibles, de liaisons et aussi de contacts avec des impacts et du frottement sec. L'avantage du formalisme présenté est à la fois un traitement consistant des sauts de vitesses dus aux impacts et une élévation automatique de l'ordre d'intégration local. Pour un traitement approprié des contraintes dans les intervalles impulsifs et non–impulsifs, les contraintes sont implicitement formulées au niveau des vitesses au moyen d'une technique de lagrangien augmenté [5]. Ces contraintes sont satisfaites de manière exacte. Pour raisons d'efficacité, toutes les autres évaluations sont explicites ce qui conduit à une méthode semi–explicite.

Le schéma numérique est un schéma étendu d'intégration en temps à la Moreau [42]. Il est basé sur des méthodes de Galerkin discontinues conservant les fonctions test d'ordre élevé des schémas d'intégration de type "event-driven" et la consistance des approches de type "time–stepping" pour la dynamique des systèmes non réguliers avec impact et frottement. Un découpage (splitting) sépare les efforts de contact impulsifs des efforts de contact non–impulsifs. Les impacts sont contenus dans les discontinuités des fonctions test linéaires par morceaux, c'est à dire, avec un précision du premier ordre. Les forces non impulsives sont integrées avec l'ordre local des fonctions test d'ordre supérieur. Pour résoudre les contraintes, un ensemble d'équations non lisses doit être résolu à chaque pas de temps suivant le nombre d'étages de la méthode. La résolution du saut de vitesses conduit à une autre équation non régulière. Toutes ces équations sont traitées par des méthodes de Newton semi–lisses.

Le schéma d'intégration au niveau des accélérations a été introduit dans [51] et dénommé "forecasting trapezoidal rule". Il a été analysé et appliqué au problème de la balle rebondissante sans tenir compte du frottement. Dans ce travail, l'algorithmie est détaillée, améliorée et appliquée à des exemples non–linéaires avec de multiplies contacts frottants. Le nouveau schéma est comparé aux autres schémas numériques et il est montré qu'il conduit à un comportement unifié de la description des problèmes de mécanique du contact.

Mots-clés : Schémas d'intégration en temps, méthodes de Galerkin discontinues, dynamique non–régulière, frottement, impact, réduction d'index

Contents

1 Introduction

In this paper, we study numerical integration schemes for the simulation of nonsmooth mechanical systems. Rigid and flexible bodies, joints as well as contacts and impacts with dry friction constitute the mechanical models. Thereby, we formulate the contact conditions as constraints and do not allow any penetration, e.g. due to penalty techniques. As a result, velocity jumps occur during the transient simulation of semi-discrete models and we have to be cautious in the formulation of efficient and stable time-discretization schemes.

We distinguish two cases.

1. *non-impulsive contact forces* – For the contact between flexible bodies, the contact force is finite in continuum models, i.e., in not semi-discrete models, although velocity jumps may arise. Classic (implicit) time integration schemes for computational mechanical problems, i.e., members of the Newmark family [45, 31, 15, 55, 8], have been adapted to these demands and extended with respect to contact/velocity updates (Laursen-Love scheme) [37, 18]. Another strategy to preferably get a well-posed problem is the application of energy-momentum paradigms like in energy-momentum schemes [56, 8], i.e., modifications of the midpoint rule [55], to impact problems (Laursen-Chawla scheme) [37]. A contact-stabilized Newmark scheme is proposed in [17].

2. *impulsive contact forces* – For the contact between rigid bodies, the reaction forces are impulsive and the classic time integration schemes do not work anymore [3]. The application of mass redistribution techniques [18] is a procedure, which reminds of penalty approaches with the benefit of having a theoretical foundation [60]. However in [36] it is shown, that all these schemes suffer from oscillations in the relative contact velocities. Event-driven schemes and timestepping schemes are further concepts to simulate rigid multibody systems or semi-discrete systems consistently by applying impact laws. Thereby, event-driven schemes resolve impact events to a high precision. In-between impact events, standard integration schemes are used. Classic timestepping schemes do not resolve impact events, but include their possible existence directly in the discretization. Thus, they have low accuracy in non-impulsive intervals, whereas event-driven schemes may get inefficient and inconsistent for many impact events [3].

The aim of the present paper is to improve the consistent and robust concept of timestepping schemes for semi-discrete mechanical systems. The main drawback is the lack of problem adaptive accuracy in non-impulsive intervals. Classic timestepping schemes can be embedded within the context of time-discontinuous Galerkin methods, when we choose piecewise constant trial functions for the velocity approximation [51]. In the aforementioned paper, two different families of timestepping schemes on acceleration level based on discontinuous Galerkin methods have been introduced and analyzed. They differ in the interpretation, if one assumes the velocity jump at the beginning, called D^+ timestepping schemes, or at the end, called D^- timestepping schemes, of each discretization interval. First, using higher-order but piecewise continuous trial functions for the velocity, and, second, splitting of impulsive and non-impulsive contact reactions, offer the opportunity to both stay consistent and benefit from a higher-order integration of non-impulsive contact reactions. The "forecasting trapezoidal rule" is the D^- representative for piecewise linear velocity trial functions; concerning function evaluations and implementation complexity it is the easiest scheme. Its basic practical applicability apart from theoretical propositions has been shown with a decoupled bouncing ball example. It is the basis for extensions in the present paper. We algorithmically specify and improve it and apply it to nonlinear multi-contact examples with friction. Thereby for an automatic switching between non-impulsive and impulsive intervals, constraint equations for non-impulsive reactions are also formulated on velocity level in an augmented Lagrangian setting [5] like the constraint equations for contact impulse and jumping velocity. Therefore, we focus on half-explicit methods and evaluate all other magnitudes but the constraints explicitly [9, 10, 43, 44, 7, 29, 30]. The number of nonsmooth equations for the constraints depends on the number of stages, i.e., the local order of the underlying trial functions. These three nonsmooth equations are solved separately by semi-smooth Newton methods [5, 14, 49].

The recent proposal for higher-order integration of non-impulsive contact reactions on basis of the generalized-α scheme [12] is also footing on a specific splitting approach. Splitting is interpreted as separating the "flow" of applied forces, bilateral contact reactions and unilateral contact reactions in the classic "Strang-sense" [41]. In contrast, we split non-impulsive and impulsive reactions not depending on their source. In particular, closed, i.e., active unilateral contacts, are treated with first-order accuracy in [12] but benefit from a higher-order approximation in the present approach.

The paper introduces the new time-discretization scheme step-by-step. The proposed (intermedi-

ate) schemes are directly evaluated using an impacting slider-crank mechanism which we introduce in Sect. 2.1. The paper is organized as follows. Section 2 introduces the equations of motion and common time-discretization schemes for nonsmooth mechanical systems. Half-explicit timestepping schemes on acceleration level are introduced in Sect. 3. They generalize the approach in [51] algorithmically but suffer from drift-off effects. In Sect. 4, a first attempt for a velocity-level approximation is discussed to reduce the drift-off effect. It follows the constraint evaluation ideas of the half-explicit timestepping schemes on acceleration level and yields an explicit but not half-explicit scheme on velocity level, with even increased drift-off effect. The final half-explicit scheme on velocity level is derived and described in Sect. 5. It is tested within the example of the slider-crank mechanism. In Sect. 6, we analyze the performance of our proposed timestepping scheme with the example of the slider-crank mechanism and a bouncing ball example. In Sect. 7, we extend this analysis to flexible systems with the examples of an elastic bar and a rotor. Section 8 concludes the paper.

2 Equations of motion and time-discretization

This section introduces the continuous equations of motion, the impacting slider-crank mechanism as an accompanying example and basic time-discretization schemes. We consider an impacting mechanical system with dry friction. For non-impulsive motion in time, it is described by the following set of equations

$$\dot{q} = v \,, \tag{1}$$

and

$$M\dot{v} = h + W_N \lambda_N + W_T \lambda_T \,, \tag{2}$$

$$0 \leq g_N \perp \lambda_N \geq 0 \,, \tag{3}$$

$$\begin{cases} \|\lambda_T\| \leq \mu \lambda_N & \text{for } \dot{g}_T = 0 \wedge g_N \leq 0 \\ \lambda_T = -\frac{\dot{g}_T}{\|\dot{g}_T\|} \mu \lambda_N & \text{for } \dot{g}_T \neq 0 \wedge g_N \leq 0 \end{cases} . \tag{4}$$

For mechanical systems, these equations typically occur after semi-discretization in space of respective mathematical models, e.g. by the finite element method [18]. If one does not use any classic concept of regularization by introducing contact stiffnesses or contact potentials [61, 21], an impact may occur at time $t_j \geq 0$ and we have to use

$$M\left(q\left(t_j\right)\right)\left(v_j^+ - v_j^-\right) = W_N\left(q\left(t_j\right)\right)\Lambda_{N,j} + W_T\left(q\left(t_j\right)\right)\Lambda_{T,j} \,, \tag{5}$$

$$0 \leq \dot{g}_{N,j}^+ + \varepsilon_N \dot{g}_{N,j}^- \perp \Lambda_{N,j} \geq 0 \,, \tag{6}$$

$$\begin{cases} \left\|\Lambda_{T,j}\right\| \leq \mu \Lambda_{N,j} & \text{for } \dot{g}_{T,j}^+ + \varepsilon_T \dot{g}_{T,j}^- = 0 \\ \Lambda_{T,j} = -\frac{\dot{g}_{T,j}^+ + \varepsilon_T \dot{g}_{T,j}^-}{\left\|\dot{g}_{T,j}^+ + \varepsilon_T \dot{g}_{T,j}^-\right\|} \mu \Lambda_{N,j} & \text{for } \dot{g}_{T,j}^+ + \varepsilon_T \dot{g}_{T,j}^- \neq 0 \end{cases} \tag{7}$$

instead of (2)-(4).

We want to calculate the generalized position and generalized velocity functions on the time interval $I := [0,T]$ with $T > 0$:

$$q \,:\, [0,T] \to \mathbb{R}^{N_d} \,,\, t \mapsto q(t) \,, \tag{8}$$

$$v \,:\, [0,T] \to \mathbb{R}^{N_d} \,,\, t \mapsto v(t) \,. \tag{9}$$

With the initial conditions

$$q(0) = q_0 \,, \tag{10}$$

$$v(0) = v_0 \,, \tag{11}$$

the evolution of q and v is non-impulsive almost everywhere due to (2)-(4).

The generalized mass matrix satisfies

$$M : \mathbb{R}^{N_d} \to \mathbb{R}^{N_d,N_d} \,,\; q \mapsto M(q) \tag{12}$$

and the nonlinear generalized force has the structure

$$h : \mathbb{R}^{N_d} \times \mathbb{R}^{N_d} \to \mathbb{R}^{N_d} \,,\; (q,v) \mapsto h(q,v) \,. \tag{13}$$

The matrices of generalized force directions W_N and W_T are the derivatives of the nonlinear normal and tangential gap functions

$$g_N \;:\; \mathbb{R}^{N_d} \to \mathbb{R}^{N_c} \,,\; q \mapsto g_N(q) \,, \tag{14}$$

$$g_T \;:\; \mathbb{R}^{N_d} \to \mathbb{R}^{N_c} \,,\; q \mapsto g_T(q) \tag{15}$$

with respect to q. These describe normal distances and tangential displacements of contacting bodies in a mechanical system and are therefore constraining its motion. The Lagrange multipliers

$$\lambda_N \;:\; [0,T] \to \mathbb{R}^{N_c} \,,\; t \mapsto \lambda_N(t) \tag{16}$$

can be identified with normal contact forces in the equality of forces (2) and in the non-penetration condition (3). The Lagrange multipliers

$$\lambda_T \;:\; [0,T] \to \mathbb{R}^{N_c} \,,\; t \mapsto \lambda_T(t) \tag{17}$$

can be identified with tangential contact forces in the equality of forces (2) and in (4), which contains sticking and sliding conditions with the friction coefficient $\mu \geq 0$ and the time-derivative denoted by a dot. The index set $\mathscr{I}_0$ contains all constraints on the system.

$$\mathscr{I}_1^q = \left\{ k \in \mathscr{I}_0 \;:\; g_{N_k}(q) \leq 0 \right\} \text{ is the continuous index set of the closed constraints} \,, \tag{18}$$

$$\mathscr{I}_2^{q,v^\pm} = \left\{ k \in \mathscr{I}_1^q \;:\; \dot{g}_{N_k}(q,v^\pm) \leq 0 \right\} \text{ is the continuous index set of the closed constraints, which stay closed} \,. \tag{19}$$

For countable time instances t_j, the evolution of the mechanical system might get impulsive, e.g. if $g_{N_{k^*}}(q(t_j)) = 0$ for some component k^*, but $g_{N_{k^*}}(q(t)) > 0$ for $t_j - \delta \leq t < t_j$ with an appropriate $\delta > 0$. The impact equations (5), Newton's impact law (6) with the coefficient of restitution $\varepsilon_N \in [0,1]$ and Newton's impact law (7) with the coefficient of restitution $\varepsilon_T \in [0,1]$ have to be solved instead of (2)-(4). This possibly leads to jumps in the velocity variables. Their derivatives do not exist anymore in the classical sense. One has to define the left-hand and right-hand limits

$$\dot{g}_{N_j}^- := \lim_{t \uparrow t_j} \dot{g}_N(t) \,, \quad \dot{g}_{T_j}^- := \lim_{t \uparrow t_j} \dot{g}_T(t) \,, \tag{20}$$

$$\dot{g}_{N_j}^+ := \lim_{t \downarrow t_j} \dot{g}_N(t) \,, \quad \dot{g}_{T_j}^+ := \lim_{t \downarrow t_j} \dot{g}_T(t) \,. \tag{21}$$

Then, the Lagrange multipliers

$$\Lambda_{N_j} = \lim_{\delta \downarrow 0} \int_{t_j - \delta}^{t_j} \lambda_N \mathrm{d}t \,, \quad \Lambda_{T_j} = \lim_{\delta \downarrow 0} \int_{t_j - \delta}^{t_j} \lambda_T \mathrm{d}t \tag{22}$$

describe the finite impulsive interaction in the sense of distributions.

Equations (1)-(7) describe impacting mechanical systems in general. Their mechanical, mathematical and numerical behaviour have been detailed in the monographs [11, 27, 3, 38, 48, 34, 58] even discussing more sophisticated impact laws of kinetic or energetic type.

2.1 Slider-crank mechanism

The slider-crank mechanism in Fig. 1 is a nonlinear benchmark example for an impacting mechanical system with dry friction. The generalized positions q consist of the angles θ_1, θ_2 and θ_3 as well as the

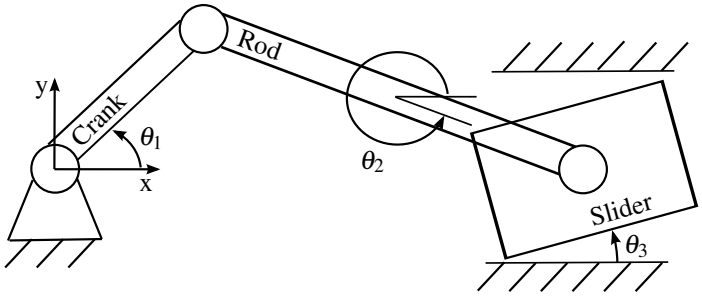

Figure 1: Slider-crank mechanism with unilateral constraints and friction [22, 54].

generalized velocities v consist of the angular velocities ω_1, ω_2 and ω_3.

The generalized mass matrix satisfies

$$M : \mathbb{R}^3 \to \mathbb{R}^{3,3}\ ,\ q \mapsto M(q) = \begin{pmatrix} J_1 + l_1^2\left(\frac{m_1}{4} + m_2 + m_3\right) & l_1 l_2 \cos(\theta_1 - \theta_2)\left(\frac{m_2}{2} + m_3\right) & 0 \\ l_1 l_2 \cos(\theta_1 - \theta_2)\left(\frac{m_2}{2} + m_3\right) & J_2 + l_2^2\left(\frac{m_2}{4} + m_3\right) & 0 \\ 0 & 0 & J_3 \end{pmatrix}, \tag{23}$$

and the nonlinear generalized force can be obtained by

$$h : \mathbb{R}^3 \times \mathbb{R}^3 \to \mathbb{R}^3\ ,\ (q,v) \mapsto h(q,v) = \begin{pmatrix} -l_1 l_2 \sin(\theta_1 - \theta_2)\left(\frac{m_2}{2} + m_3\right)\omega_2^2 - \gamma l_1 \cos\theta_1\left(\frac{m_1}{2} + m_2 + m_3\right) \\ l_1 l_2 \sin(\theta_1 - \theta_2)\left(\frac{m_2}{2} + m_3\right)\omega_1^2 - \gamma l_2 \cos\theta_2\left(\frac{m_2}{2} + m_3\right) \\ 0 \end{pmatrix}. \tag{24}$$

Thereby, it is l_1 the length of the crank and l_2 the length of the connecting rod. The inertia of crank, connecting rod and slider consist of translational masses, i.e., m_1, m_2 and m_3, as well as of rotational inertia values, i.e., J_1, J_2 and J_3. The system is subject to gravitation γ.

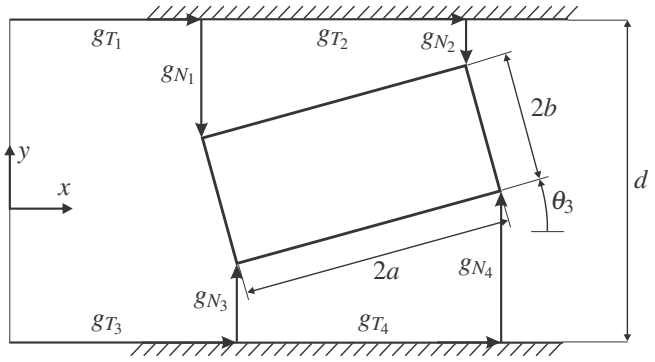

Figure 2: Definition of the gap functions for the slider-crank mechanism with unilateral constraints and friction [22].

Considering the geometry of the slider according to Fig. 2, the nonlinear normal and tangential gap functions split up for each corner:

$$g_{N_1}(q) = \frac{d}{2} - l_1 \sin\theta_1 - l_2 \sin\theta_2 + a\sin\theta_3 - b\cos\theta_3 \,, \tag{25}$$

$$g_{N_2}(q) = \frac{d}{2} - l_1 \sin\theta_1 - l_2 \sin\theta_2 - a\sin\theta_3 - b\cos\theta_3 \,, \tag{26}$$

$$g_{N_3}(q) = \frac{d}{2} + l_1 \sin\theta_1 + l_2 \sin\theta_2 - a\sin\theta_3 - b\cos\theta_3 \,, \tag{27}$$

$$g_{N_4}(q) = \frac{d}{2} + l_1 \sin\theta_1 + l_2 \sin\theta_2 + a\sin\theta_3 - b\cos\theta_3 \,, \tag{28}$$

$$g_{T_1}(q) = l_1 \cos\theta_1 + l_2 \cos\theta_2 - a\cos\theta_3 - b\sin\theta_3 \,, \tag{29}$$

$$g_{T_2}(q) = l_1 \cos\theta_1 + l_2 \cos\theta_2 + a\cos\theta_3 - b\sin\theta_3 \,, \tag{30}$$

$$g_{T_3}(q) = l_1 \cos\theta_1 + l_2 \cos\theta_2 - a\cos\theta_3 + b\sin\theta_3 \,, \tag{31}$$

$$g_{T_4}(q) = l_1 \cos\theta_1 + l_2 \cos\theta_2 + a\cos\theta_3 + b\sin\theta_3 \,. \tag{32}$$

It is $2a$ the length and $2b$ the height of the slider. The height of the notch is given by d and the gap can be defined by c. The matrices of generalized force directions are given by

$$W_N : \mathbb{R}^3 \to \mathbb{R}^{3,4} \,,\; q \mapsto W_N(q) = \begin{pmatrix} -l_1\cos\theta_1 & -l_2\cos\theta_2 & a\cos\theta_3 + b\sin\theta_3 \\ -l_1\cos\theta_1 & -l_2\cos\theta_2 & -a\cos\theta_3 + b\sin\theta_3 \\ l_1\cos\theta_1 & l_2\cos\theta_2 & -a\cos\theta_3 + b\sin\theta_3 \\ l_1\cos\theta_1 & l_2\cos\theta_2 & a\cos\theta_3 + b\sin\theta_3 \end{pmatrix}^T \,, \tag{33}$$

$$W_T : \mathbb{R}^3 \to \mathbb{R}^{3,4} \,,\; q \mapsto W_T(q) = \begin{pmatrix} -l_1\sin\theta_1 & -l_2\sin\theta_2 & a\sin\theta_3 - b\cos\theta_3 \\ -l_1\sin\theta_1 & -l_2\sin\theta_2 & -a\sin\theta_3 - b\cos\theta_3 \\ -l_1\sin\theta_1 & -l_2\sin\theta_2 & a\sin\theta_3 + b\cos\theta_3 \\ -l_1\sin\theta_1 & -l_2\sin\theta_2 & -a\sin\theta_3 + b\cos\theta_3 \end{pmatrix}^T \,. \tag{34}$$

Only the i-th column of the matrix $\frac{\partial W_N^T}{\partial q_i} \in \mathbb{R}^{4,3}$ does not vanish. We summarize this information in the matrix

$$Q_N = \begin{pmatrix} l_1\sin\theta_1 & l_2\sin\theta_2 & -a\sin\theta_3 + b\cos\theta_3 \\ l_1\sin\theta_1 & l_2\sin\theta_2 & a\sin\theta_3 + b\cos\theta_3 \\ -l_1\sin\theta_1 & -l_2\sin\theta_2 & a\sin\theta_3 + b\cos\theta_3 \\ -l_1\sin\theta_1 & -l_2\sin\theta_2 & -a\sin\theta_3 + b\cos\theta_3 \end{pmatrix} \tag{35}$$

and define

$$v_\blacksquare = \begin{pmatrix} v_1^2 & v_2^2 & v_3^2 \end{pmatrix}^T \,. \tag{36}$$

Fixed characteristics used in this work are given in Table 1.

We focus on numerical integration and therefore point out particular previous work just in this direction. Classically, we distinguish event-driven respectively event-tracking schemes and timestepping respectively event-capturing schemes.

2.2 Event-driven schemes

An event-driven scheme discretizes the non-impulsive equations (1)-(4) by a classic numerical rule [3, Chap. 8]. At the same time, it observes the gap functions for open ($g_N > 0$)-close ($g_N \leq 0$) transitions

Geometrical characteristics	$l_1 = 0.1530\,\mathrm{m}$
	$l_2 = 0.3060\,\mathrm{m}$
	$a = 0.0500\,\mathrm{m}$
	$b = 0.0250\,\mathrm{m}$
	$c = 0.0010\,\mathrm{m}$
Inertia properties	$m_1 = 0.0380\,\mathrm{kg}$
	$m_2 = 0.0380\,\mathrm{kg}$
	$m_3 = 0.0760\,\mathrm{kg}$
	$J_1 = 7.4 \cdot 10^{-5}\,\mathrm{kgm}^2$
	$J_2 = 5.9 \cdot 10^{-4}\,\mathrm{kgm}^2$
	$J_3 = 2.7 \cdot 10^{-6}\,\mathrm{kgm}^2$
Force elements	$\gamma = 9.81\,\mathrm{m/s}^2$
Contact parameters	$\varepsilon_{N_1} = \varepsilon_{N_2} = \varepsilon_{N_3} = \varepsilon_{N_4} = 0.4$
	$\varepsilon_{T_1} = \varepsilon_{T_2} = \varepsilon_{T_3} = \varepsilon_{T_4} = 0.0$
	$\mu_1 = \mu_2 = \mu_3 = \mu_4 = 0.01$
Initial conditions	$\theta_{1_0} = 0.0$
	$\theta_{2_0} = 0.0$
	$\theta_{3_0} = 0.0$
	$\omega_{1_0} = 150.01/\mathrm{s}$
	$\omega_{2_0} = -75.01/\mathrm{s}$
	$\omega_{3_0} = 0.01/\mathrm{s}$

Table 1: Characteristics of the slider-crank mechanism with unilateral constraints and friction [22, 54].

or stick ($\dot{g}_T = 0$)-slip ($\dot{g}_T \neq 0$) transitions. In such cases, the exact transition time is resolved by a root-finding algorithm with respect to a given tolerance because the structure, i.e., the actual degree of freedom of the mathematical model, changes and therefore also the numerical discretization has to be adapted. In the case of an open-close transition, the impact equations (5)-(7) have to be solved separately and subsequently the non-impulsive integration has to be restarted. LSODAR[1] for index 0 or DASKR[2] for index 2 formulations are typical examples for the derivation of the numerical model by standard integration schemes. Thereby, the relation of the index of the non-impulsive equations (1)-(4) and of their numerical counterpart play a crucial part for the discretization [19, 30]. We discuss this concept for timestepping schemes in the following subsection. As event-driven schemes resolve the exact transition times, they, first, cannot resolve Zeno phenomena, i.e., an infinite number of impacts in a finite time interval. Second, even the resolution of the transition time itself may be crucial as the used tolerance is depending on the specific mechanical problem, e.g. on penetration velocities. These are two main drawbacks of event-driven schemes for their application to the mathematical description of impacting mechanical systems. However for non-impulsive intervals, event-driven schemes are extremely efficient because they are based on sophisticated numerical integration schemes with e.g. high accuracy for the numerical representation of the non-impulsive equations.

2.3 Classic timestepping schemes

Classic timestepping schemes do not distinguish impulsive and non-impulsive equations, i.e., they do not resolve exact transition times. Hence, no additional tolerances are required. Classic timestepping schemes discretize the equations of motion including the constraints, impact laws and impact equations

[1] http://www.netlib.org/odepack/
[2] http://www.netlib.org/ode/

in a physically consistent and uniform way [3, Chap. 10]. This means that possible impacts are the determining factor for the order of classic timestepping schemes. In comparison to the maximum possible order in non-impulsive phases, the actual order may be low. However, convergence results are available for classic timestepping schemes and not for event-driven schemes. Two mainstream concepts for classic timestepping schemes exist: Schatzman-Paoli [46, 47] and Moreau-Jean schemes [42, 33]. The Schatzman-Paoli scheme discretizes normal gap functions on the level of positions and satisfies impact laws after several time steps. That is why, we prefer to formulate the impact law on the level of velocities in discrete time, which is the core of Moreau-Jean schemes.

To exemplary formulate the classic explicit Moreau-Jean scheme, we construct the approximations at time t_i

$$q_i \approx q(t_i) \ , \tag{37}$$

$$v_i^- \approx \lim_{t \uparrow t_i} v(t) \ , \quad v_i^+ \approx \lim_{t \downarrow t_i} v(t) \ , \tag{38}$$

$$\Lambda_{N_i} \approx \sum_{j:t_j \in I_i} \Lambda_{N,j} \ , \quad \Lambda_{T_i} \approx \sum_{j:t_j \in I_i} \Lambda_{T,j} \tag{39}$$

and use them in the abbreviations

$$M_i^{-1} := M^{-1}(q_i) \ , \tag{40}$$

$$h_i^{\pm} := h\left(q_i, v_i^{\pm}\right) \ , \tag{41}$$

$$W_{N_i} := W_N(q_i) \ , W_{T_i} := W_T(q_i) \ . \tag{42}$$

Then, the classic explicit Moreau-Jean scheme on an arbitrary time interval $I_i := [t_{i-1}, t_i)$ with the time step-size $\Delta t_i := t_i - t_{i-1}$ is given by

$$q_i = q_{i-1} + \Delta t_i v_{i-1}^+ \ , \tag{43}$$

$$v_i^+ = v_{i-1}^+ + \Delta t_i M_{i-1}^{-1} h_{i-1}^+ + M_i^{-1} \left[W_{N_i} \Lambda_{N_i} + W_{T_i} \Lambda_{T_i} \right] \tag{44}$$

together with the active normal impact equations on velocity level

$$\Lambda_{N_i, \mathscr{I}_{1,M}^i} - \mathrm{proj}_{\mathbb{R}_0^+} \left(\Lambda_{N_i, \mathscr{I}_{1,M}^i} - r(\dot{g}^+_{N_i, \mathscr{I}_{1,M}^i} + \varepsilon_N \dot{g}^+_{N_{i-1}, \mathscr{I}_{1,M}^i}) \right) = 0 \tag{45}$$

and the active tangential impact equations on velocity level

$$\Lambda_{T_i, \mathscr{I}_{1,M}^i} - \mathrm{proj}_{C_T(\Lambda_{N_i, \mathscr{I}_{1,M}^i})} \left(\Lambda_{T_i, \mathscr{I}_{1,M}^i} - r(\dot{g}^+_{T_i, \mathscr{I}_{1,M}^i} + \varepsilon_T \dot{g}^+_{T_{i-1}, \mathscr{I}_{1,M}^i}) \right) = 0 \, . \tag{46}$$

To simplify the nonlinearity, usually one estimates active contact equations in advance by checking if a prediction, e.g. the leapfrog rule, is negative:

$$\mathscr{I}_{1,M}^i := \left\{ k \in \mathscr{I}_0 \ : \ \tilde{g}_{N_k}^i := g_{N_k}(q_{i-1}) + \frac{\Delta t}{2} \dot{g}_{Nk}(q_{i-1}, v_{i-1}^+) \leq 0 \right\} \ . \tag{47}$$

We have used the projection to a convex set C as a special case of proximations [50] to equivalently transform complementarity formulations for normal and tangential contacts. It has to be interpreted row-by-row [53]:

$$\mathrm{proj}_C : \mathbb{R} \to \mathbb{R} \ , \ x \mapsto \mathrm{proj}_C(x) = \arg\min_{x^* \in C} \|x - x^*\| \ . \tag{48}$$

The convex set to describe dry friction is the friction disc with the local normal force as radius:

$$C_T : \mathbb{R} \to \mathscr{P}\left(\mathbb{R}^2\right) : y \mapsto C_T(y) = \left\{x \in \mathbb{R}^2 \mid \|x\| \leq \mu |y|\right\} . \tag{49}$$

The parameter $r > 0$ is mathematically arbitrary. It physically transforms units and can also be interpreted as a stabilization in an augmented Lagrangian setting [5]. Therefore, it can be used to improve convergence of numerical solution schemes, which are applied to solve (43)-(46) for the unknowns q_i, v_i^+, $\Lambda_{N_i,\mathscr{I}^i_{1,M}}$ and $\Lambda_{T_i,\mathscr{I}^i_{1,M}}$. The classic explicit Moreau-Jean scheme does not adapt the time step-size and naturally combines non-impulsive and impulsive equations, contacts as well as impacts by calculating implicitly the finite mean impulses $\Lambda_{N_i,\mathscr{I}^i_{1,M}}$ and $\Lambda_{T_i,\mathscr{I}^i_{1,M}}$ within I_i; their trajectory within I_i in this sense is an assumption. Hence, several extensions are of possible interest and are current research topics:

- Constraint stabilization [54, 1, 12]
  Moreau-Jean schemes in general are formulated on the level of velocities. Hence, a linear drift-off effect from the non-penetration invariant will occur [24, 6]. The Gear-Gupta-Leimkuhler formulation [25] treats the non-penetration invariant as additional constraint and therefore inserts a derivative projection; applied to Moreau's timestepping interpretation of the midpoint rule [42], this can be understood as a symmetric projection [28, 55].

- High-frequency damping [13, 12]
  Artificial high-frequency oscillations occur due to finite element discretizations and e.g. excitation in contact problems. One possible remedy is applying the generalized-α method [15] in the sense of timestepping schemes.

- Variational integration [35]
  Sophisticated integration schemes can often be derived from a discrete variational principle [40]. This concept is tried to be extended to timestepping schemes for impacting mechanical systems. However, some kind of splitting seems to be necessary because a symplectic method will not stay symplectic for an impact event [57].

- Higher order timestepping and step-size adaptation
  There are two types of higher order timestepping schemes which can consistently deal with impacts.

  – Augmented timestepping schemes [59, 32]
    Within an augmented timestepping scheme, one applies classic augmentation strategies like order extrapolation whenever one heuristically expects no impacts during an integration step. Extrapolation induces instabilities in closed contacts because of chattering in Aitken-Neville schemes or because of the absence of splitting of non-impulsive and impulsive force propagations. It is conceptional a serial process. That is why, usually one applies a fixed increased order when we anticipate a non-impulsive phase. Also from a practical point of view, i.e., not infinitely-differentiable input data, an extrapolation-based augmentation strategy like in [39] seems to be over-designed.

  – Mixed timestepping schemes [2, 51, 20]
    A mixed timestepping scheme couples standard integration methods for non-impulsive differential algebraic equations with timestepping schemes for impulsive phases usually by heuristics.

    We extend [51] to multi-contact problems with friction. In [51], heuristics for switching between impulsive and non-impulsive phases can be avoided by embedding in discontinuous Galerkin methods. The synchronization of fixed increased order integration and consistent low order integration is automatic but as we will see perhaps not the most robust way for an implementation.

Step size adaptation can be applied for both higher order timestepping strategies. It extends the classic approach [16, 30] by heuristics which meet the timestepping idea. We mention foreseeing gap-estimations, retrospective time-step bisection, time-step size switching maintaining the overall integration order and error estimation based on Richardson extrapolation. For the latter, one could exclude velocities, discuss appropriate norms, separate impacts interval-by-interval or include the penetration depth of closed contacts. However to the knowledge of the authors, these strategies have not been theoretically analyzed in the literature.

3 Half-explicit timestepping schemes on acceleration level

This section generalizes timestepping schemes based on discontinuous Galerkin methods [51] to multi-contact examples and shows their advantages and disadvantages. The theoretical benefit of these schemes over mixed timestepping schemes is that they do not rely on heuristics. Thereby as in [51], we start by introducing contact forces on acceleration level and by splitting non-impulsive and impulsive force propagation. We try to get some experience with linear trial functions for the velocity discretization, i.e., half-explicit "forecasting" trapezoidal rules, not regarding friction:

$$q_{i-1,0} = q_{i-1} \,, \tag{50}$$

$$q_{i-1,1} = q_{i-1} + \frac{\Delta t_i}{2}\left\{v_{i-1,0} + v_{i-1,1}\right\} \,, \tag{51}$$

$$q_i = q_{i-1} + \frac{\Delta t_i}{2}\left\{v_{i-1,0} + v_{i-1,1}\right\} \,, \tag{52}$$

$$v_{i-1,0} = v_{i-1}^+ \,, \tag{53}$$

$$v_{i-1,1} = v_{i-1}^+ + \Delta t_i M_{i-1}^{-1}\left[h_{i-1}^+ + W_{N_{i-1}}\lambda_{N_{i-1}}^+\right] \,, \tag{54}$$

$$v_i^+ = v_{i-1}^+ + \frac{\Delta t_i}{2} M_{i-1}^{-1}\left[h_{i-1}^+ + W_{N_{i-1}}\lambda_{N_{i-1}}^+\right] + \frac{\Delta t_i}{2} M_{i-1,1}^{-1}\left[h_{i-1,1} + W_{N_{i-1,1}}\lambda_{N_i}^-\right] + M_i^{-1} W_{N_i}\Lambda_{N_i} \tag{55}$$

together with the active contact equations on acceleration level

$$\lambda^+_{N_{i-1},\mathscr{I}_2^{(i-1),0}} - \mathrm{proj}_{\mathbb{R}_0^+}\left[\lambda^+_{N_{i-1},\mathscr{I}_2^{(i-1),0}} - r\ddot{g}^+_{N_{i-1},\mathscr{I}_2^{(i-1),0}}\right] = 0 \,, \tag{56}$$

$$\lambda^-_{N_i,\mathscr{I}_2^{(i-1),1}} - \mathrm{proj}_{\mathbb{R}_0^+}\left[\lambda^-_{N_i,\mathscr{I}_2^{(i-1),1}} - r\ddot{g}^-_{N_i,\mathscr{I}_2^{(i-1),1}}\right] = 0 \tag{57}$$

and the active impact equations on velocity level similar to (45) but referring to another index set, which we have to define. It is

$$\mathscr{I}_1^{i,l} = \left\{k \in \mathscr{I}_0 \,:\, g_{N_k}(q_{i,l}) \le 0\right\} \text{ the discrete index set of the closed constraints} \,, \tag{58}$$

$$\mathscr{I}_2^{i,l\pm} = \left\{k \in \mathscr{I}_1^{i,l} \,:\, \dot{g}_{N_k}(q_{i,l}, v_{i,l}^\pm) \le 0\right\} \text{ the discrete index set of the closed constraints, which stay closed} \,, \tag{59}$$

and

$$\lambda_{N_i}^- \approx \lim_{t\uparrow t_i} \lambda_N(t) \,, \quad \lambda_{N_i}^+ \approx \lim_{t\downarrow t_i} \lambda_N(t) \,. \tag{60}$$

Now, what is *active* for this half-explicit trapezoidal rule? We assume that the generalized position q_{i-1} and the right-hand limit of the generalized velocity v_{i-1}^+ are known at t_{i-1} as illustrated in the graphical

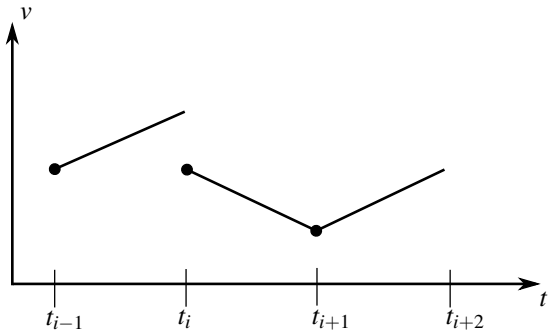

Figure 3: Interpretation of velocity jumps [54].

interpretation in Fig. 3. These values are set to the first stage of the generalized position (50) and of the generalized velocity (53), respectively. The generalized velocity is assumed to be continuous in the interior of the time interval. In the specific case of linear trial functions, there is a linear velocity propagation until its left-hand limit $v_{i-1,1}$ at t_i. Hence, the second stage (54) of the generalized velocity is calculated with a step of the explicit Euler method. Everything is known but for the right-hand limit of the contact force $\lambda^+_{N_{i-1}}$. We postpone the question whether to incorporate (56) for its calculation. From a general point of view subsequently, the second stage of the generalized position at t_i is calculated with the trapezoidal rule (51). As the jump at t_i occurs in such a way that the generalized velocity at t_i is right-continuous, the left-hand limit of the generalized velocity v_i^- is corrected by a velocity jump leading to the right-hand limit of the generalized velocity v_i^+. The respective trapezoidal rule (55) involves the unknown left-hand limit of the contact force $\lambda^-_{N_i}$ and the impulse Λ_{N_i} as well as (57) and (45) if necessary. The effects of all impulses that would technically occur in the interior of the time interval are summarized at the end of the time interval.

The procedure of incorporating (56)-(57) and (45) can be implemented straightforward for a decoupled bouncing ball example (cf. Sect. 6.2 for gravitational acceleration in $-y$-direction) because there is only one single contact possibility [51]:

- If on the one side $g_{N_{i-1}} \leq 0$ at the beginning of the time interval, we will not consider the impulse $\Lambda_{N_i} = 0$ at the end of the time interval to take advantage of higher order integration possibilities. If also $\dot{g}^+_{N_{i-1}} > 0$, it is $\lambda^+_{N_{i-1}} = 0$. Otherwise, Equation (56) is *active* for the explicit evaluation of $\lambda^+_{N_{i-1}}$ with a root-finding algorithm. Thereby, we substitute the circumstantial local acceleration because of (2):

$$\ddot{g}^+_{N_{i-1}} := W^T_{N_{i-1}} \dot{v}^+_{i-1} = W^T_{N_{i-1}} M^{-1}_{i-1} h^+_{i-1} + W^T_{N_{i-1}} M^{-1}_{i-1} W_{N_{i-1}} \lambda^+_{N_{i-1}} \,. \tag{61}$$

  If additionally $g_{N_{i-1,1}} > 0$ or $\dot{g}_{N_{i-1,1}} > 0$, it is $\lambda^-_{N_i} = 0$. Otherwise, Equation (57) is *active* for the explicit evaluation of $\lambda^-_{N_i}$ with a root-finding algorithm and the local acceleration

$$\ddot{g}^-_{N_i} := W^T_{N_{i-1,1}} \dot{v}^-_i = W^T_{N_{i-1,1}} M^{-1}_{i-1,1} h_{i-1,1} + W^T_{N_{i-1,1}} M^{-1}_{i-1,1} W_{N_{i-1,1}} \lambda^-_{N_i} \,. \tag{62}$$

- If on the other side $g_{N_{i-1}} > 0$ at the beginning of the time interval, clearly $\lambda^+_{N_{i-1}} = 0$. However, we will not consider the contact force $\lambda^-_{N_i} = 0$ at the end of the time interval because analytically it does not exist during an impact. Concerning the impulse, the additional condition $g_{N_{i-1,1}} > 0$ yields $\Lambda_{N_i} = 0$. Otherwise, Equation (45) is *active* for the implicit solution of both v_i^+ and Λ_{N_i} with a root-finding algorithm and the local velocity

$$\dot{g}^+_{N_i} := W^T_{N_i} v^+_i = \dot{g}^-_{N_i} + W^T_{N_i} M^{-1}_i W_{N_i} \Lambda_{N_i} \tag{63}$$

according to (5).

For the decoupled bouncing ball example, the proposed half-explicit trapezoidal rule works quite well and shows the expected characteristics in numerical experiments, i.e., first order accuracy in impulsive phases and second order accuracy in non-impulsive phases [51]. For multi-contact situations it is not clear how to decide which contacts shall be considered *active* concerning the three different constraint equations (56)-(57) and (45). The half-explicit trapezoidal rule needs further interpretation for a consistent extension to simultaneous contact occurrences and nonlinear dynamics.

3.1 Calculation of contact forces on acceleration level

It seems not to be a bad idea to use (3) together with (2) for the calculation of a contact force λ_N at a certain time also for more general nonlinear mechanical systems. We again interpret (3) on acceleration level

$$\lambda_N = \begin{cases} 0 & \text{if } g_N > 0 \ \vee \ \dot{g}_N > 0 \\ \text{proj}_{\mathbb{R}_0^+}\left[\lambda_N - r\ddot{g}_N\right] & \text{else} \end{cases} \tag{64}$$

using the projection-formulation row-by-row. Often, we have to deal with holonomic-scleronomic constraints:

$$\dot{g}_N = W_N^T v \,, \tag{65}$$

$$\ddot{g}_N = \underbrace{\dot{W}_N^T}_{\sum_i \frac{\partial W_N^T}{\partial q_i} v_i} v + W_N^T \dot{v} \,. \tag{66}$$

We can simplify (66) to

$$\ddot{g}_N = Q_N v_\blacksquare + W_N^T \dot{v} \tag{67}$$

with $v_\blacksquare$ containing squared generalized velocity combinations. In comparison to the decoupled bouncing ball example, the *nonlinearity* in (67) and in the right-hand side h newly arises. As before, we eliminate $\dot{v}$ in (67) by using (2):

$$\ddot{g}_N = Q_N v_\blacksquare + W_N^T M^{-1} h + G_N \lambda_N \tag{68}$$

with the Delassus matrix [38], i.e., the mass action matrix [48],

$$G_N = W_N^T M^{-1} W_N \,. \tag{69}$$

We focus on active contacts, $\mathscr{I}_2$ on acceleration level, and transform (64) formally using row-by-row interpretation:

$$\lambda_{N,\mathscr{I}_2} = \text{proj}_{\mathbb{R}_0^+}\left[\lambda_{N,\mathscr{I}_2} - r(\underbrace{Q_{N,\mathscr{I}_2} v_\blacksquare + W_{N,\mathscr{I}_2}^T M^{-1} h + G_{N,\mathscr{I}_2}\lambda_{N,\mathscr{I}_2}}_{\ddot{g}_{N,\mathscr{I}_2}})\right] \,. \tag{70}$$

In the multi-contact case, active contacts might be *depending*. Hence if we decide to use e.g. a semi-smooth Newton method as root-finding algorithm to solve (70), we have to switch to semi-smooth variants

of the Gauss-Newton method. This means that we systematically have to choose an approximate root $\bar{\lambda}_{N,\mathscr{I}_2}$ of the function

$$f : \mathbb{R}^{|\mathscr{I}_2|} \to \mathbb{R}^{|\mathscr{I}_2|} \, , \, \lambda_{N,\mathscr{I}_2} \mapsto f(\lambda_{N,\mathscr{I}_2}) = \lambda_{N,\mathscr{I}_2} - \mathrm{proj}_{\mathbb{R}_0^+}\left[\lambda_{N,\mathscr{I}_2} - r\ddot{g}_{N,\mathscr{I}_2}(\lambda_{N,\mathscr{I}_2})\right] \tag{71}$$

with the Moore-Penrose pseudoinverse operator pinv. The Gauss-Newton algorithm reads

$$\begin{aligned}
&\bar{\lambda}_{N,\mathscr{I}_2} = 0 \, , \, \bar{f} = f(\bar{\lambda}_{N,\mathscr{I}_2}) \\
&\text{while } \left\|\bar{f}\right\| > \mathrm{TOL} \\
&\quad \nabla f(\bar{\lambda}_{N,\mathscr{I}_2}) = I - \Theta\left[\bar{\lambda}_{N,\mathscr{I}_2} - r\ddot{g}_{N,\mathscr{I}_2}(\bar{\lambda}_{N,\mathscr{I}_2})\right](I - rG_{N,\mathscr{I}_2}) \\
&\quad \bar{\lambda}_{N_{new},\mathscr{I}_2} = \bar{\lambda}_{N,\mathscr{I}_2} - \mathrm{pinv}(\nabla f(\bar{\lambda}_{N,\mathscr{I}_2}))\bar{f} \\
&\quad \bar{\lambda}_{N,\mathscr{I}_2} = \bar{\lambda}_{N_{new},\mathscr{I}_2} \\
&\quad \bar{f} = f(\bar{\lambda}_{N,\mathscr{I}_2}) \\
&\text{end}
\end{aligned} \tag{72}$$

The occurring Heaviside function

$$\Theta : \mathbb{R} \to \mathbb{R} \, , \, x \mapsto \Theta(x) = \begin{cases} 0 & \text{if } x < 0 \\ 1 & \text{else} \end{cases} \tag{73}$$

is interpreted row-by-row and we use a fixed parameter r [53].

3.2 Smooth position and velocity prediction

After having calculated the right-hand limit of the contact force $\lambda_{N_{i-1}}^+$ at t_{i-1} according to Sect. 3.1, we predict the left-hand limit of the generalized velocity at t_i, i.e., the second stage of the generalized velocity:

$$v_{i-1,1} = v_{i-1}^+ + \Delta t_i M_{i-1}^{-1}\left[h_{i-1}^+ + W_{N_{i-1}}\lambda_{N_{i-1}}^+\right] \, . \tag{74}$$

Subsequently, we calculate the second stage of the generalized position:

$$q_{i-1,1} = q_{i-1} + \frac{\Delta t_i}{2}\left\{v_{i-1,0} + v_{i-1,1}\right\} \, . \tag{75}$$

3.3 Assignment of contact forces and impulses

Now, we have a pair of generalized position and generalized velocity at the left-hand limit of t_i that allows us to calculate the gap function g_{N_i}.

- If on the one hand there is no gap function which has been inactive ($g_{N_{k^*}}\left(q_{i-1,0}\right) > 0$) at t_{i-1} and which now becomes active ($g_{N_{k^*}}\left(q_{i-1,1}\right) \leq 0$) at t_i, no impact has to be considered. We set $\Lambda_{N_i} = 0$ to fully profit of higher integration possibilities and calculate the left-hand limit of the contact force $\lambda_{N_i}^-$ at t_i according to Sect. 3.1. Knowing $\lambda_{N_i}^-$, we improve the predicted left-hand limit of the generalized velocity at t_i:

$$v_i^- := v_{i-1}^+ + \frac{\Delta t_i}{2} M_{i-1}^{-1}\left[h_{i-1}^+ + W_{N_{i-1}}\lambda_{N_{i-1}}^+\right] + \frac{\Delta t_i}{2} M_{i-1,1}^{-1}\left[h_{i-1,1} + W_{N_{i-1,1}}\lambda_{N_i}^-\right] \, . \tag{76}$$

- If on the other hand there is at least one inactive gap function ($g_{N_{k^*}}\left(q_{i-1,0}\right) > 0$) at t_{i-1} that now becomes active ($g_{N_{k^*}}\left(q_{i-1,1}\right) \leq 0$), an impact occurs in the whole rigidly connected component of the impact source. Hence in this *rigidly connected component*, the calculation of $\lambda_{N_i}^-$ is not consistent and does not improve the accuracy of the scheme. For the ease of description, we set $\lambda_{N_i}^- = 0$ and also $\lambda_{N_{i-1}}^+ = 0$ everywhere in the multibody system and calculate the left-hand limit of the generalized velocity at t_i, i.e., the free velocity:

$$v_i^- := v_{i-1}^+ + \frac{\Delta t_i}{2}\left\{M_{i-1}^{-1}h_{i-1}^+ + M_{i-1,1}^{-1}h_{i-1,1}\right\} . \tag{77}$$

This global consequence does not occur in the decoupled bouncing ball example. For the computation of v_i^+ and Λ_{N_i}, we write (6) on velocity level row-by-row:

$$\Lambda_{N_i} = \begin{cases} 0 & \text{if } g_N\left(q_{i-1,1}\right) > 0 \\ \operatorname{proj}_{\mathbb{R}_0^+}\left[\Lambda_{N_i} - r(\underbrace{\dot{g}_{N_i}^+ + \varepsilon_N \dot{g}_{N_i}^-}_{\dot{\bar{g}}_{N_i}^+})\right] & \text{else} \end{cases} . \tag{78}$$

Equation (5) can be used to eliminate $\dot{g}_{N_i}^+$, row-by-row resulting in

$$\Lambda_{N_i,\mathscr{I}_1^{i-1,1}} = \operatorname{proj}_{\mathbb{R}_0^+}\left[\Lambda_{N_i,\mathscr{I}_1^{i-1,1}} - r(\underbrace{G_{N_i,\mathscr{I}_1^{i-1,1}}\Lambda_{N_i,\mathscr{I}_1^{i-1,1}} + (I+\varepsilon_{N,\mathscr{I}_1^{i-1,1}})W_{N_i,\mathscr{I}_1^{i-1,1}}^T v_i^-}_{\dot{\bar{g}}_{N_i,\mathscr{I}_1^{i-1,1}}^+})\right] \tag{79}$$

with $G_{N_i} := G_N(q_i)$. We look for the roots of

$$f : \mathbb{R}^{|\mathscr{I}_1^{i-1,1}|} \to \mathbb{R}^{|\mathscr{I}_1^{i-1,1}|} , \Lambda_{N_i,\mathscr{I}_1^{i-1,1}} \mapsto f(\Lambda_{N_i,\mathscr{I}_1^{i-1,1}}) = \Lambda_{N_i,\mathscr{I}_1^{i-1,1}} - \operatorname{proj}_{\mathbb{R}_0^+}\left[\Lambda_{N_i,\mathscr{I}_1^{i-1,1}} - r\dot{\bar{g}}_{N_i,\mathscr{I}_1^{i-1,1}}^+\right] \tag{80}$$

with a semi-smooth Gauss-Newton method as in (72). The derivative of f at $\Lambda_{N_i,\mathscr{I}_1^{i-1,1}}$ is given by

$$\nabla f(\Lambda_{N_i,\mathscr{I}_1^{i-1,1}}) = I - \Theta\left[\Lambda_{N_i,\mathscr{I}_1^{i-1,1}} - r\dot{\bar{g}}_{N_i,\mathscr{I}_1^{i-1,1}}^+\right](I - rG_{N_i,\mathscr{I}_1^{i-1,1}}) . \tag{81}$$

We have to use structures from classic timestepping schemes and event-driven schemes to define the half-explicit trapezoidal rule.

3.4 State increment

Finally, we update the generalized velocity:

$$v_i^+ = v_i^- + M_i^{-1}W_{N_i}\Lambda_{N_i} . \tag{82}$$

Hence in the impact-free case, it is $v_i^+ = v_i^-$ as expected. For the generalized position, it is

$$q_i = q_{i-1} + \frac{\Delta t_i}{2}\left\{v_{i-1,0} + v_{i-1,1}\right\} . \tag{83}$$

Specify characteristics, start time $t = 0$, end time T, time step size Δt

Initialize $i = 1$
For $t < T$
Evaluate left-hand side
Evaluate $q_{i-1,0} = q_{i-1}$ (50)
Evaluate $v_{i-1,0} = v_{i-1}^+$ (53)
Evaluate $\lambda_{N_{i-1}}^+$ on acceleration level ($\mathscr{I}_2^{(i-1),0}$)

Predict right-hand side
Compute $v_{i-1,1} = v_{i-1}^+ + \Delta t_i M_{i-1}^{-1} \left[h_{i-1}^+ + W_{N_{i-1}} \lambda_{N_{i-1}}^+ \right]$ (54)
Compute $q_{i-1,1} = q_{i-1} + \frac{\Delta t_i}{2} \{ v_{i-1,0} + v_{i-1,1} \}$ (51)

Decide strategy
if $\nexists k^* : g_{N_{k^*}} \left(q_{i-1,0} \right) > 0 \wedge g_{N_{k^*}} \left(q_{i-1,1} \right) \leq 0$ (14)
Set $\Lambda_{N_i} = 0$
Evaluate $\lambda_{N_i}^-$ on acceleration level ($\mathscr{I}_2^{(i-1),1}$)
Compute $v_i^- = v_{i-1}^+ + \frac{\Delta t_i}{2} M_{i-1}^{-1} \left[h_{i-1}^+ + W_{N_{i-1}} \lambda_{N_{i-1}}^+ \right] + \frac{\Delta t_i}{2} M_{i-1,1}^{-1} \left[h_{i-1,1} + W_{N_{i-1,1}} \lambda_{N_i}^- \right]$ (76)
if $\exists k^* : g_{N_{k^*}} \left(q_{i-1,0} \right) > 0 \wedge g_{N_{k^*}} \left(q_{i-1,1} \right) \leq 0$ (14)
Set $\lambda_{N_{i-1}}^+ = 0$ and $\lambda_{N_i}^- = 0$
Compute $v_i^- = v_{i-1}^+ + \frac{\Delta t_i}{2} \left\{ M_{i-1}^{-1} h_{i-1}^+ + M_{i-1,1}^{-1} h_{i-1,1} \right\}$ (77)
Compute Λ_{N_i} on velocity level ($\mathscr{I}_1^{i-1,1}$)

State increment
Compute $v_i^+ = v_i^- + M_i^{-1} W_{N_i} \Lambda_{N_i}$ (82)
Compute $q_i = q_{i-1} + \frac{\Delta t_i}{2} \{ v_{i-1,0} + v_{i-1,1} \}$ (83)

Write result of time step, e.g. q_i and v_i^+

Update t by Δt_i and increment i by 1

Postprocessing

Figure 4: Flowchart of the half-explicit timestepping scheme on acceleration level.

3.5 Overview

The overall algorithm can be summarized as shown in Fig. 4.

3.6 First analysis of simulation results

Simulation results for the slider-crank mechanism in Fig. 1 of Sect. 2.1 with $\varepsilon_N = 0.4$ and $\Delta t = 10^{-4}$ s are depicted in Figs. 5 and 6. The curves show a nearly perfect behavior. The benefits from the time-discontinuous Galerkin schemes presented in [51] concerning theoretical investigations and a decoupled bouncing ball example can also be carried over to multi-contact examples. Impulsive and non-impulsive periods are seperated; hence, higher-order trial functions can be used in non-impulsive periods whereas consistency is preserved for the impacts. Nevertheless, we improve the curves concerning the following observations. The penetration of the bordering wall occurs because timestepping schemes in general do not detect but only capture events, e.g. the time instant when a gap function closes. Contact activity means $g_{N_{i,l}} \leq 0 \ \wedge \ \dot{g}_{N_{i,l}}^{\pm} \leq 0$ and not $g_{N_{i,l}} = 0 \ \wedge \ \dot{g}_{N_{i,l}}^{\pm} = 0$. We will see that a velocity level discretization

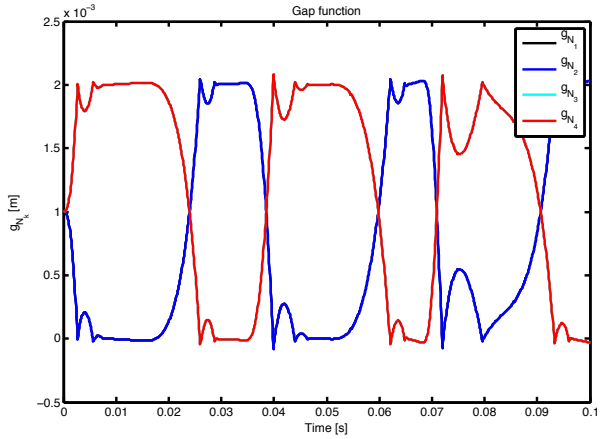

Figure 5: Normal gap functions of the slider for half-explicit timestepping on acceleration level.

of the contact forces is a remedy for the drift-off effect and opens the path to include friction naturally. On acceleration level, the implementation of the friction transitions would also be rather complicated. On velocity level, the nonlinearity in the equations of motion, e.g. $v_{\blacksquare}$, will be reduced. Nonlinearity in general induces the not always decreasing energy trend of the trapezoidal rule which differs from the midpoint rule in the nonlinear regime [55]. On acceleration level, contacts and impacts are defined by different activity rules using $\mathscr{I}_2$ and $\mathscr{I}_1$. As a compromise between acceleration and position level discretizations, the velocity level discretization will unify contact and impact activation rules.

4 Explicit timestepping schemes on velocity level

In this section, we reduce the drawbacks, i.e., the degree of nonlinearity and the drift-off effect, for half-explicit timestepping schemes on velocity level from the preceding section by introducing a velocity level discretization:

$$q_{i-1,0} = q_{i-1} \,, \tag{84}$$

$$q_{i-1,1} = q_{i-1} + \frac{\Delta t_i}{2}\left\{v_{i-1,0} + v_{i-1,1}\right\} \,, \tag{85}$$

$$q_i = q_{i-1} + \frac{\Delta t_i}{2}\left\{v_{i-1,0} + v_{i-1,1}\right\} \,, \tag{86}$$

$$v_{i-1,0} = v_{i-1}^+ \,, \tag{87}$$

$$v_{i-1,1} = v_{i-1}^+ + \Delta t_i M_{i-1}^{-1}\left[h_{i-1}^+ + W_{N_{i-1}}\lambda_{N_{i-1}}^+ + W_{T_{i-1}}\lambda_{T_{i-1}}^+\right] \,, \tag{88}$$

$$\begin{aligned} v_i^+ = v_{i-1}^+ &+ \frac{\Delta t_i}{2} M_{i-1}^{-1}\left[h_{i-1}^+ + W_{N_{i-1}}\lambda_{N_{i-1}}^+ + W_{T_{i-1}}\lambda_{T_{i-1}}^+\right] + \frac{\Delta t_i}{2} M_{i-1,1}^{-1}\left[h_{i-1,1} + W_{N_{i-1,1}}\lambda_{N_i}^- + W_{T_{i-1,1}}\lambda_{T_i}^-\right] \\ &+ M_i^{-1}\left[W_{N_i}\Lambda_{N_i} + W_{T_i}\Lambda_{T_i}\right] \end{aligned} \tag{89}$$

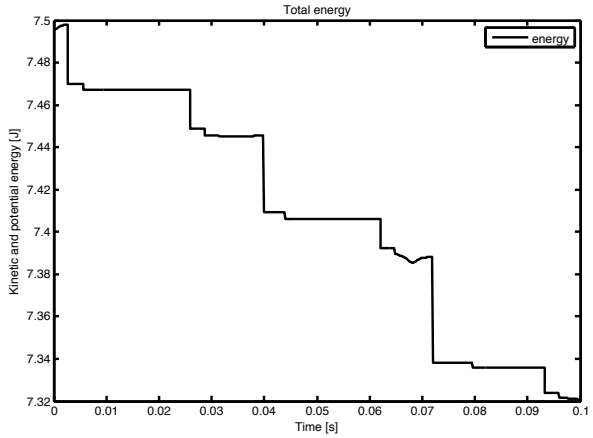

Figure 6: Total energy of the slider-crank mechanism for half-explicit timestepping on acceleration level.

together with the active normal contact equations on velocity level

$$\lambda^{+}_{N_{i-1},\mathscr{I}_1^{i-1,0}} - \mathrm{proj}_{\mathbb{R}^{+}_{0}}\left(\lambda^{+}_{N_{i-1},\mathscr{I}_1^{i-1,0}} - r\dot{g}^{+}_{N_{i-1},\mathscr{I}_1^{i-1,0}}\right) = 0\,, \tag{90}$$

$$\lambda^{-}_{N_{i},\mathscr{I}_1^{i-1,1}} - \mathrm{proj}_{\mathbb{R}^{+}_{0}}\left(\lambda^{-}_{N_{i},\mathscr{I}_1^{i-1,1}} - r\dot{g}_{N_{i-1,1},\mathscr{I}_1^{i-1,1}}\right) = 0 \tag{91}$$

and the active normal impact equations on velocity level (78). Then, we can easily include friction which naturally is stated on velocity level. For the active tangential contact equations on velocity level, we get

$$\lambda^{+}_{T_{i-1},\mathscr{I}_1^{i-1,0}} - \mathrm{proj}_{C_T(\lambda^{+}_{N_{i-1},\mathscr{I}_1^{i-1,0}})}\left(\lambda^{+}_{T_{i-1},\mathscr{I}_1^{i-1,0}} - r\dot{g}^{+}_{T_{i-1},\mathscr{I}_1^{i-1,0}}\right) = 0\,, \tag{92}$$

$$\lambda^{-}_{T_{i},\mathscr{I}_1^{i-1,1}} - \mathrm{proj}_{C_T(\lambda^{-}_{N_{i},\mathscr{I}_1^{i-1,1}})}\left(\lambda^{-}_{T_{i},\mathscr{I}_1^{i-1,1}} - r\dot{g}_{T_{i-1,1},\mathscr{I}_1^{i-1,1}}\right) = 0 \tag{93}$$

with

$$\lambda^{-}_{T_i} \approx \lim_{t\uparrow t_i}\lambda_T(t)\,, \quad \lambda^{+}_{T_i} \approx \lim_{t\downarrow t_i}\lambda_T(t)\,. \tag{94}$$

The active tangential impact equations on velocity level are similar to (46).

4.1 Calculation of contact forces on velocity level

As in Sect. 3.1, we use (3) and (4) together with (2) for the calculation of contact forces λ_N and λ_T. We interpret (3) and (4) on velocity level

$$\lambda_N = \begin{cases} 0 & \text{if } g_N > 0 \\ \mathrm{proj}_{\mathbb{R}^{+}_{0}}\left[\lambda_N - r\dot{g}_N\right] & \text{else} \end{cases}, \tag{95}$$

$$\lambda_T = \begin{cases} 0 & \text{if } g_N > 0 \\ \mathrm{proj}_{C_T(\lambda_N)}\left[\lambda_T - r\dot{g}_T\right] & \text{else} \end{cases} \tag{96}$$

using the projection-formulation row-by-row. Thereby now in contrast to Sect. 3.1, the necessary local kinematics

$$\dot{g}_N = W_N^T v \,, \quad \dot{g}_T = W_T^T v \tag{97}$$

is already known and we cannot directly calculate the contact forces with (95), (96). Hence, we start calculating equivalent forces λ_N and λ_T such that the given local velocities are projected into their respective admissible space, e.g. during one time step – which is an assumption of an *explicit representation*. That is why, we substitute

$$\dot{g}_{N,\mathrm{proj}} = \dot{g}_N + \Delta t \left\{ W_N^T M^{-1} \tilde{h} + G_N \lambda_N + W_N^T M^{-1} W_T \lambda_T \right\} \,, \tag{98}$$

$$\dot{g}_{T,\mathrm{proj}} = \dot{g}_T + \Delta t \left\{ W_T^T M^{-1} \tilde{h} + W_T^T M^{-1} W_N \lambda_N + G_T \lambda_T \right\} \tag{99}$$

in (3) and (4) using

$$\tilde{h} : \mathbb{R}^{N_d} \times \mathbb{R}^{N_d} \to \mathbb{R}^{N_d} \,,\ (q,v) \mapsto \tilde{h}(q,v) = \begin{cases} h(q,v) & \text{option 1: more implicit trend} \\ 0 & \text{option 2: less implicit trend} \end{cases} . \tag{100}$$

Thereby, it is

$$G_N = W_N^T M^{-1} W_N \,, \quad G_T = W_T^T M^{-1} W_T \,. \tag{101}$$

We again focus on active contacts and transform (95) and (96) formally using row-by-row interpretation:

$$\lambda_{N,\mathscr{I}_1} = \mathrm{proj}_{\mathbb{R}_0^+} \left[\lambda_{N,\mathscr{I}_1} - r \dot{g}_{N,\mathrm{proj},\mathscr{I}_1}(\lambda_{N,\mathscr{I}_1}, \lambda_{T,\mathscr{I}_1}) \right] \,, \tag{102}$$

$$\lambda_{T,\mathscr{I}_1} = \mathrm{proj}_{C_T(\lambda_{N,\mathscr{I}_1})} \left[\lambda_{T,\mathscr{I}_1} - r \dot{g}_{T,\mathrm{proj},\mathscr{I}_1}(\lambda_{N,\mathscr{I}_1}, \lambda_{T,\mathscr{I}_1}) \right] \,. \tag{103}$$

As in Sect. 3.1, we exemplary choose a semi-smooth variant of the Gauss-Newton method, i.e., we systematically select an approximate root $\left(\bar{\lambda}_{N,\mathscr{I}_1}, \bar{\lambda}_{T,\mathscr{I}_1}\right)$ of the function

$$\begin{aligned} f : \mathbb{R}^{|\mathscr{I}_1|} \times \mathbb{R}^{2|\mathscr{I}_1|} \to \mathbb{R}^{|\mathscr{I}_1|} \times \mathbb{R}^{2|\mathscr{I}_1|} \,,\ \left(\lambda_{N,\mathscr{I}_1}, \lambda_{T,\mathscr{I}_1}\right) \mapsto f(\lambda_{N,\mathscr{I}_1}, \lambda_{T,\mathscr{I}_1}) \\ = \begin{pmatrix} \lambda_{N,\mathscr{I}_1} - \mathrm{proj}_{\mathbb{R}_0^+} \left[\lambda_{N,\mathscr{I}_1} - r \dot{g}_{N,\mathrm{proj},\mathscr{I}_1}(\lambda_{N,\mathscr{I}_1}, \lambda_{T,\mathscr{I}_1}) \right] \\ \lambda_{T,\mathscr{I}_1} - \mathrm{proj}_{C_T(\lambda_{N,\mathscr{I}_1})} \left[\lambda_{T,\mathscr{I}_1} - r \dot{g}_{T,\mathrm{proj},\mathscr{I}_1}(\lambda_{N,\mathscr{I}_1}, \lambda_{T,\mathscr{I}_1}) \right] \end{pmatrix} \end{aligned} \tag{104}$$

with the Moore-Penrose pseudoinverse operator pinv. The Gauss-Newton algorithm reads

$$\begin{aligned} &\left(\bar{\lambda}_{N,\mathscr{I}_1}, \bar{\lambda}_{T,\mathscr{I}_1}\right) = (0,0) \ ,\ \bar{f} = f\left(\bar{\lambda}_{N,\mathscr{I}_1}, \bar{\lambda}_{T,\mathscr{I}_1}\right) \\ &\text{while } \left\|\bar{f}\right\| > \mathrm{TOL} \\ &\quad \nabla f\left(\bar{\lambda}_{N,\mathscr{I}_1}, \bar{\lambda}_{T,\mathscr{I}_1}\right) = \begin{pmatrix} I & 0 \\ 0 & I \end{pmatrix} - \begin{pmatrix} \Theta_N(I - r\Delta t G_{N,\mathscr{I}_1}) & \Theta_N(-r\Delta t W_{N,\mathscr{I}_1}^T M^{-1} W_{T,\mathscr{I}_1}) \\ \Theta_T(-r\Delta t (W_{T,\mathscr{I}_1}^T M^{-1} W_{N,\mathscr{I}_1}) & \Theta_T(I - r\Delta t G_{T,\mathscr{I}_1}) \end{pmatrix} \\ &\quad \left(\bar{\lambda}_{N_{\mathrm{new}},\mathscr{I}_1}, \bar{\lambda}_{T_{\mathrm{new}},\mathscr{I}_1}\right) = \left(\bar{\lambda}_{N,\mathscr{I}_1}, \bar{\lambda}_{T,\mathscr{I}_1}\right) - \mathrm{pinv}(\nabla f\left(\bar{\lambda}_{N,\mathscr{I}_1}, \bar{\lambda}_{T,\mathscr{I}_1}\right))\bar{f} \\ &\quad \left(\bar{\lambda}_{N,\mathscr{I}_1}, \bar{\lambda}_{T,\mathscr{I}_1}\right) = \left(\bar{\lambda}_{N_{\mathrm{new}},\mathscr{I}_1}, \bar{\lambda}_{T_{\mathrm{new}},\mathscr{I}_1}\right) \\ &\quad \bar{f} = f\left(\bar{\lambda}_{N,\mathscr{I}_1}, \bar{\lambda}_{T,\mathscr{I}_1}\right) \\ &\text{end} \end{aligned} \tag{105}$$

The occurring Heaviside functions

$$\Theta_N : \mathbb{R}^{|\mathscr{I}_1|} \times \mathbb{R}^{2|\mathscr{I}_1|} \to \mathrm{diag}^{|\mathscr{I}_1|,|\mathscr{I}_1|} \, , \, \Theta_{N_{kk}}\left(\lambda_{N,\mathscr{I}_1}, \lambda_{T,\mathscr{I}_1}\right) = \begin{cases} 0 & \text{if } \lambda_{N_k} - r\dot{g}_{N_k,\mathrm{proj}} < 0 \\ 1 & \text{else} \end{cases} , \tag{106}$$

$$\Theta_T : \mathbb{R}^{|\mathscr{I}_1|} \times \mathbb{R}^{2|\mathscr{I}_1|} \to \mathrm{diag}^{|\mathscr{I}_1|,|\mathscr{I}_1|} \, , \, \Theta_{T_{kk}}\left(\lambda_{N,\mathscr{I}_1}, \lambda_{T,\mathscr{I}_1}\right) = \begin{cases} 0 & \text{if } \left\|\lambda_{T_k} - r\dot{g}_{T_k,\mathrm{proj}}\right\| > \mu \left|\lambda_{N_k}\right| \\ 1 & \text{else} \end{cases} . \tag{107}$$

are interpreted row-by-row and we use a fixed parameter r.

4.2 Smooth position and velocity prediction

According to the acceleration level case, we predict the left-hand limit of the generalized velocity at t_i, which now also includes the friction contribution:

$$v_{i-1,1} = v_{i-1}^+ + \Delta t_i M_{i-1}^{-1}\left[h_{i-1}^+ + W_{N_{i-1}}\lambda_{N_{i-1}}^+ + W_{T_{i-1}}\lambda_{T_{i-1}}^+\right] . \tag{108}$$

Subsequently, we calculate the second stage of the generalized position with (75).

4.3 Assignment of contact forces and impulses

With the gap function $g_{N_{i-1,1}}$, we can distinguish non-impulsive and impulsive phases.

- Non-impulsive:

$$v_i^- = v_{i-1}^+ + \frac{\Delta t_i}{2} M_{i-1}^{-1}\left[h_{i-1}^+ + W_{N_{i-1}}\lambda_{N_{i-1}}^+ + W_{T_{i-1}}\lambda_{T_{i-1}}^+\right] + \frac{\Delta t_i}{2} M_{i-1,1}^{-1}\left[h_{i-1,1} + W_{N_{i-1,1}}\lambda_{N_i}^- + W_{T_{i-1,1}}\lambda_{T_i}^-\right] . \tag{109}$$

- Impulsive:
  We remind of the free velocity (77) and of (6) in its row-by-row description (78). Then, we write also (7) on velocity level row-by-row:

$$\Lambda_{T_i} = \begin{cases} 0 & \text{if } g_{N_{i-1,1}} > 0 \\ \mathrm{proj}_{C_T(\Lambda_{N_i})}\left[\Lambda_{T_i} - r(\underbrace{\dot{g}_{T_i}^+ + \varepsilon_T \dot{g}_{T_i}^-}_{\dot{\tilde{g}}_{T_i}^+})\right] & \text{else} \end{cases} . \tag{110}$$

  Elimination of $\dot{\tilde{g}}_{N_i}^+$ and $\dot{\tilde{g}}_{T_i}^+$ for active contacts on position level includes friction contributions:

$$\Lambda_{N_i,\mathscr{I}_1^{i-1,1}} = \mathrm{proj}_{\mathbb{R}_0^+}\left[\Lambda_{N_i,\mathscr{I}_1^{i-1,1}} - r\dot{\tilde{g}}_{N_i,\mathscr{I}_1^{i-1,1}}\right] , \tag{111}$$

$$\Lambda_{T_i,\mathscr{I}_1^{i-1,1}} = \mathrm{proj}_{C_T(\Lambda_{N_i,\mathscr{I}_1^{i-1,1}})}\left[\Lambda_{T_i,\mathscr{I}_1^{i-1,1}} - r\dot{\tilde{g}}_{T_i,\mathscr{I}_1^{i-1,1}}\right] . \tag{112}$$

  We solve for $\left(\Lambda_{N,\mathscr{I}_1}, \Lambda_{T,\mathscr{I}_1}\right)$ as roots of a summarizing function

$$f : \mathbb{R}^{|\mathscr{I}_1|} \times \mathbb{R}^{2|\mathscr{I}_1|} \to \mathbb{R}^{|\mathscr{I}_1|} \times \mathbb{R}^{2|\mathscr{I}_1|} \tag{113}$$

  with a semi-smooth Gauss-Newton method.

4.4 State increment

Finally, we update the generalized velocity by

$$v_i^+ = v_i^- + M_i^{-1}\left(W_{N_i}\Lambda_{N_i} + W_{T_i}\Lambda_{T_i}\right) \tag{114}$$

and the generalized position by (83).

4.5 Overview

Specify characteristics, start time $t = 0$, end time T, time step size Δt
Initialize $i = 1$ For $t < T$ *Evaluate left-hand side* Evaluate $q_{i-1,0} = q_{i-1}$ (50) Evaluate $v_{i-1,0} = v_{i-1}^+$ (53) Evaluate $\lambda_{N_{i-1}}^+$, $\lambda_{T_{i-1}}^+$ on velocity level $(\mathscr{I}_1^{i-1,0})$
Predict right-hand side Compute $v_{i-1,1} = v_{i-1}^+ + \Delta t_i M_{i-1}^{-1}\left[h_{i-1}^+ + W_{N_{i-1}}\lambda_{N_{i-1}}^+ + W_{T_{i-1}}\lambda_{T_{i-1}}^+\right]$ (54) Compute $q_{i-1,1} = q_{i-1} + \frac{\Delta t_i}{2}\left\{v_{i-1,0} + v_{i-1,1}\right\}$ (51)
Decide strategy if $\nexists k^* : g_{N_{k^*}}\left(q_{i-1,0}\right) > 0 \wedge g_{N_{k^*}}\left(q_{i-1,1}\right) \leq 0$ (14) Set $\Lambda_{N_i} = 0$, $\Lambda_{T_i} = 0$ Evaluate $\lambda_{N_i}^-$, $\lambda_{T_i}^-$ on velocity level $(\mathscr{I}_1^{i-1,1})$ Compute $v_i^- = v_{i-1}^+ + \frac{\Delta t_i}{2} M_{i-1}^{-1}\left[h_{i-1}^+ + W_{N_{i-1}}\lambda_{N_{i-1}}^+ + W_{T_{i-1}}\lambda_{T_{i-1}}^+\right] + \frac{\Delta t_i}{2} M_{i-1,1}^{-1}\left[h_{i-1,1} + W_{N_{i-1,1}}\lambda_{N_i}^- + W_{T_{i-1,1}}\lambda_{T_i}^-\right]$ (109) if $\exists k^* : g_{N_{k^*}}\left(q_{i-1,0}\right) > 0 \wedge g_{N_{k^*}}\left(q_{i-1,1}\right) \leq 0$ (14) Set $\lambda_{N_{i-1}}^+ = 0$, $\lambda_{T_{i-1}}^+ = 0$ and $\lambda_{N_i}^- = 0$, $\lambda_{T_i}^- = 0$ Compute $v_i^- = v_{i-1}^+ + \frac{\Delta t_i}{2}\left\{M_{i-1}^{-1} h_{i-1}^+ + M_{i-1,1}^{-1} h_{i-1,1}\right\}$ (77) Compute Λ_{N_i}, Λ_{T_i} on velocity level $(\mathscr{I}_1^i)$
State increment Compute $v_i^+ = v_i^- + M_i^{-1}\left(W_{N_i}\Lambda_{N_i} + W_{T_i}\Lambda_{T_i}\right)$ (114) Compute $q_i = q_{i-1} + \frac{\Delta t_i}{2}\left\{v_{i-1,0} + v_{i-1,1}\right\}$ (83)
Write result of time step, e.g. q_i and v_i^+
Update t by Δt_i and increment i by 1
Postprocessing

Figure 7: Flowchart of the explicit timestepping scheme on velocity level.

The overall algorithm can be summarized as shown in Fig. 7.

4.6 Second analysis of simulation results

Simulation results of the slider-crank mechanism in Fig. 1 of Sect. 2.1 with $\varepsilon_N = 0.4$, $\Delta t = 10^{-4}$ s and $\tilde{h} \equiv 0$ are depicted in Fig. 8. The drift-off effect is quite strong, even stronger than for the half-explicit

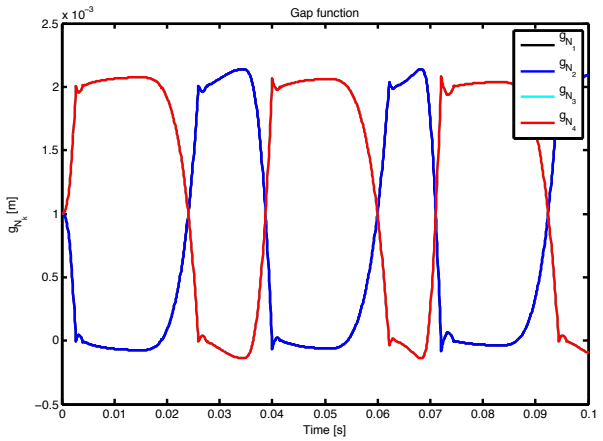

Figure 8: Normal gap functions of the slider for explicit timestepping on velocity level.

acceleration level approach. The choice $\tilde{h} \equiv h$ additionally induces bad oscillatory behavior into the nonlinear slider-crank mechanism, i.e., loss of contact which even cannot be resolved by keeping the activation rule from the left to the right interval end ($\mathscr{I}_1^{i-1,1} = \mathscr{I}_1^{i-1,0}$, not shown). An implicit calculation of the contact forces is proposed as a remedy.

5 Half-explicit timestepping schemes on velocity level

This section introduces the final version of the proposed schemes by correctly applying velocity level discretizations in an implicit way and hence reducing the degree of nonlinearity and the drift-off effect from half-explicit timestepping schemes on acceleration level (Sect. 3). Using an implicit evaluation of constraints [9, 10, 43, 44, 7, 29, 30], we do not have a projection anymore as in (98) and (99) for calculating both $\lambda^+_{N_{i-1}}$, $\lambda^+_{T_{i-1}}$ and $\lambda^-_{N_i}$, $\lambda^-_{T_i}$. Instead, we solve the following equations for the second stage of the velocity

$$0 = \lambda^+_{N_{i-1},\mathscr{I}_1^{i-1,0}} - \mathrm{proj}_{\mathrm{IR}_0^+}\left(\lambda^+_{N_{i-1},\mathscr{I}_1^{i-1,0}} - rW^T_{N,\mathscr{I}_1^{i-1,0}}(q_{i-1} + \Delta t_i v^+_{i-1})v_{i-1,1}\right), \tag{115}$$

$$0 = \lambda^+_{T_{i-1},\mathscr{I}_1^{i-1,0}} - \mathrm{proj}_{C_T(\lambda^+_{N_{i-1},\mathscr{I}_1^{i-1,0}})}\left(\lambda^+_{T_{i-1},\mathscr{I}_1^{i-1,0}} - rW^T_{T,\mathscr{I}_1^{i-1,0}}(q_{i-1} + \Delta t_i v^+_{i-1})v_{i-1,1}\right) \tag{116}$$

and the following equations assuming that the output equation of the trapezoidal rule defines a virtual third stage:

$$0 = \lambda^-_{N_i,\mathscr{I}_1^{i-1,1}} - \mathrm{proj}_{\mathrm{IR}_0^+}\left(\lambda^-_{N_i,\mathscr{I}_1^{i-1,1}} - rW^T_{N_i,\mathscr{I}_1^{i-1,1}} v^-_i\right), \tag{117}$$

$$0 = \lambda^-_{T_i,\mathscr{I}_1^{i-1,1}} - \mathrm{proj}_{C_T(\lambda^-_{N_i,\mathscr{I}_1^{i-1,1}})}\left(\lambda^-_{T_i,\mathscr{I}_1^{i-1,1}} - rW^T_{T_i,\mathscr{I}_1^{i-1,1}} v^-_i\right). \tag{118}$$

It is important to evaluate W on the right-hand side of the interval. As we do not know its value for the second stage of the velocity, we have to calculate a prediction, which, however, is not used for the

calculation of any index set. The virtual third stage of the velocity coincides with the output equation of the trapezoidal rule. Hence, the velocity level constraint is automatically satisfied also for the beginning of the next time step. The overall algorithm can be summarized as shown in Fig. 9.

Specify characteristics, start time $t = 0$, end time T, time step size Δt

Initialize $i = 1$

For $t < T$

Evaluate left-hand side

Evaluate $q_{i-1,0} = q_{i-1}$ (50)

Evaluate $v_{i-1,0} = v_{i-1}^{+}$ (53)

Predict right-hand side

Compute Lagrange multipliers on velocity level

$$\lambda^{+}_{N_{i-1},\mathscr{I}_1^{i-1,0}} - \mathrm{proj}_{\mathbb{R}_0^+}\left(\lambda^{+}_{N_{i-1},\mathscr{I}_1^{i-1,0}} - rW^{T}_{N,\mathscr{I}_1^{i-1,0}}(q_{i-1}+\Delta t_i v^{+}_{i-1})v_{i-1,1}\right) = 0$$

$$\lambda^{+}_{T_{i-1},\mathscr{I}_1^{i-1,0}} - \mathrm{proj}_{C_T(\lambda^{+}_{N_{i-1},\mathscr{I}_1^{i-1,0}})}\left(\lambda^{+}_{T_{i-1},\mathscr{I}_1^{i-1,0}} - rW^{T}_{T,\mathscr{I}_1^{i-1,0}}(q_{i-1}+\Delta t_i v^{+}_{i-1})v_{i-1,1}\right) = 0$$

with $v_{i-1,1} = v^{+}_{i-1} + \Delta t_i M^{-1}_{i-1}\left[h^{+}_{i-1} + W_{N_{i-1}}\lambda^{+}_{N_{i-1}} + W_{T_{i-1}}\lambda^{+}_{T_{i-1}}\right]$

Compute $q_{i-1,1} = q_{i-1} + \frac{\Delta t_i}{2}\left\{v_{i-1,0} + v_{i-1,1}\right\}$ (51)

Decide strategy

if $\nexists k^* : g_{N_{k^*}}\left(q_{i-1,0}\right) > 0 \wedge g_{N_{k^*}}\left(q_{i-1,1}\right) \leq 0$ (14)

Set $\Lambda_{N_i} = 0$, $\Lambda_{T_i} = 0$

Compute Lagrange multipliers on velocity level

$$\lambda^{-}_{N_i,\mathscr{I}_1^{i-1,1}} - \mathrm{proj}_{\mathbb{R}_0^+}\left(\lambda^{-}_{N_i,\mathscr{I}_1^{i-1,1}} - rW^{T}_{N_i,\mathscr{I}_1^{i-1,1}}v_i^{-}\right) = 0$$

$$\lambda^{-}_{T_i,\mathscr{I}_1^{i-1,1}} - \mathrm{proj}_{C_T(\lambda^{-}_{N_i,\mathscr{I}_1^{i-1,1}})}\left(\lambda^{-}_{T_i,\mathscr{I}_1^{i-1,1}} - rW^{T}_{T_i,\mathscr{I}_1^{i-1,1}}v_i^{-}\right) = 0$$

with $v_i^{-} = v^{+}_{i-1} + \frac{\Delta t_i}{2}M^{-1}_{i-1}\left[h^{+}_{i-1} + W_{N_{i-1}}\lambda^{+}_{N_{i-1}} + W_{T_{i-1}}\lambda^{+}_{T_{i-1}}\right] + \frac{\Delta t_i}{2}M^{-1}_{i-1,1}\left[h_{i-1,1} + W_{N_{i-1,1}}\lambda^{-}_{N_i} + W_{T_{i-1,1}}\lambda^{-}_{T_i}\right]$

if $\exists k^* : g_{N_{k^*}}\left(q_{i-1,0}\right) > 0 \wedge g_{N_{k^*}}\left(q_{i-1,1}\right) \leq 0$ (14)

Set $\lambda^{+}_{N_{i-1}} = 0$, $\lambda^{+}_{T_{i-1}} = 0$ and $\lambda^{-}_{N_i} = 0$, $\lambda^{-}_{T_i} = 0$

Compute $v_i^{-} = v^{+}_{i-1} + \frac{\Delta t_i}{2}\left\{M^{-1}_{i-1}h^{+}_{i-1} + M^{-1}_{i-1,1}h_{i-1,1}\right\}$ (77)

Compute $\Lambda_{N_i}, \Lambda_{T_i}$ on velocity level $(\mathscr{I}_1^{i-1,1})$

State increment

Compute $v_i^{+} = v_i^{-} + M_i^{-1}\left(W_{N_i}\Lambda_{N_i} + W_{T_i}\Lambda_{T_i}\right)$ (82)

Compute $q_i = q_{i-1} + \frac{\Delta t_i}{2}\left\{v_{i-1,0} + v_{i-1,1}\right\}$ (83)

Write result of time step, e.g. q_i and v_i^{+}

Update t by Δt_i and increment i by 1

Postprocessing

Figure 9: Flowchart of the half-explicit timestepping scheme on velocity level.

5.1 Third analysis of simulation results

With the half-explicit evaluation of the constraints, we get the typical results of a velocity level discretization in comparison to the acceleration level discretization (Fig. 10) discussing the slider-crank mechanism in Fig. 1 of Sect. 2.1 with $\varepsilon_N = 0.4$ and $\Delta t = 10^{-4}$ s.

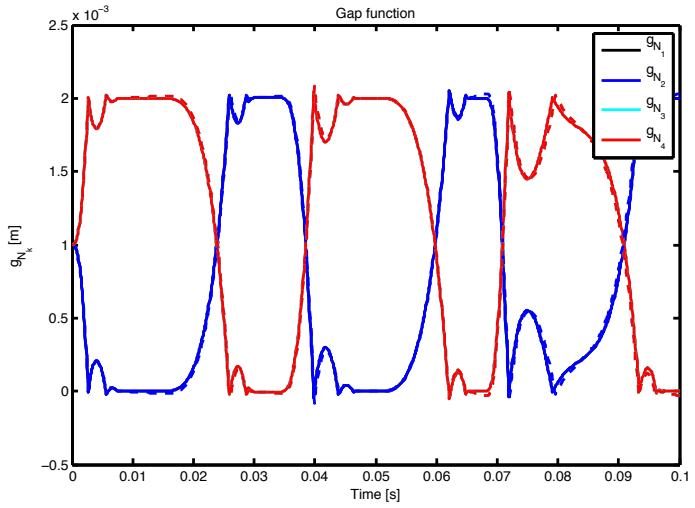

Figure 10: Normal gap functions of the slider for half-explicit timestepping on acceleration (dotted) and velocity level (solid).

5.2 Half-explicit timestepping schemes on velocity level in the sense of [9]

For the half-explicit trapezoidal rule, we just adapt the interpretation of how to evaluate the constraints. Hence, we keep the interpretation as a time-discontinuous Galerkin method. However, we can also interpret the scheme with the notation of [9]:

$$q_{i-1,0} = q_{i-1} \,, \tag{119}$$

$$q_{i-1,1} = q_{i-1} + \Delta t_i v^+_{i-1} \,, \tag{120}$$

$$v_{i-1,0} = v^+_{i-1} \,, \tag{121}$$

$$v_{i-1,1} = v^+_{i-1} + \Delta t_i M^{-1}_{i-1} \left[h^+_{i-1} + W_{N_{i-1}} \lambda^+_{N_{i-1}} + W_{T_{i-1}} \lambda^+_{T_{i-1}} \right] \,, \tag{122}$$

$$0 = \lambda^+_{N_{i-1},\mathscr{I}_1^{i-1,0}} - \mathrm{proj}_{\mathbb{R}^+_0} \left(\lambda^+_{N_{i-1},\mathscr{I}_1^{i-1,0}} - r W^T_{N,\mathscr{I}_1^{i-1,0}}(q_{i-1,1}) v_{i-1,1} \right) \,, \tag{123}$$

$$0 = \lambda^+_{T_{i-1},\mathscr{I}_1^{i-1,0}} - \mathrm{proj}_{C_T(\lambda^+_{N_{i-1},\mathscr{I}_1^{i-1,0}})} \left(\lambda^+_{T_{i-1},\mathscr{I}_1^{i-1,0}} - r W^T_{T,\mathscr{I}_1^{i-1,0}}(q_{i-1,1}) v_{i-1,1} \right) \tag{124}$$

for the first stage unknowns $v_{i-1,1}$, $\lambda^+_{N_{i-1}}$ and $\lambda^+_{T_{i-1}}$. For this interpretation, we have to change (120), e.g. to a forward Euler step. Then, we proceed:

$$q_i = q_{i-1} + \frac{\Delta t_i}{2}\left\{v_{i-1,0} + v_{i-1,1}\right\} , \tag{125}$$

$$v_i^- = v_{i-1}^+ + \frac{\Delta t_i}{2} M_{i-1}^{-1}\left[h_{i-1}^+ + W_{N_{i-1}}\lambda^+_{N_{i-1}} + W_{T_{i-1}}\lambda^+_{T_{i-1}}\right] + \frac{\Delta t_i}{2} M_i^{-1}\left[h(q_i, v_{i-1,1}) + W_{N_i}\lambda^-_{N_i} + W_{T_i}\lambda^-_{T_i}\right] , \tag{126}$$

$$0 = \lambda^-_{N_i,\mathscr{I}_1^i} - \mathrm{proj}_{\mathbb{R}_0^+}\left(\lambda^-_{N_i,\mathscr{I}_1^i} - rW^T_{N_i,\mathscr{I}_1^i} v_i^-\right) , \tag{127}$$

$$0 = \lambda^-_{T_i,\mathscr{I}_1^i} - \mathrm{proj}_{C_T(\lambda^-_{N_i,\mathscr{I}_1^i})}\left(\lambda^-_{T_i,\mathscr{I}_1^i} - rW^T_{T_i,\mathscr{I}_1^i} v_i^-\right) . \tag{128}$$

The unknowns for the second stage are v_i^-, $\lambda^-_{N_i}$ and $\lambda^-_{T_i}$. As an option, we can evaluate the impact equations without taking care, because they are also stated on velocity level and, as the case may be, automatically satisfied. Concerning efficient evaluations, however, we implement a robust procedure as shown in Fig. 9.

$$v_i^+ = v_i^- + M_i^{-1}\left[W_{N_i}\Lambda_{N_i} + W_{T_i}\Lambda_{T_i}\right] , \tag{129}$$

$$0 = \Lambda_{N_i,\mathscr{I}_1^i} - \mathrm{proj}_{\mathbb{R}_0^+}\left[\Lambda_{N_i} - r\dot{\tilde{g}}_{N_i,\mathscr{I}_1^i}\right] , \tag{130}$$

$$0 = \Lambda_{T_i,\mathscr{I}_1^i} - \mathrm{proj}_{C_T(\Lambda_{N_i})}\left[\Lambda_{T_i} - r\dot{\tilde{g}}_{T_i,\mathscr{I}_1^i}\right] . \tag{131}$$

The unknowns are v_i^+, Λ_{N_i} and Λ_{T_i}.

The "forecasting trapezoidal rule" is the easiest member of D^+ or D^- timestepping schemes [51]. For the other representatives the internal stages for position and velocity as well as their corresponding constraint equations are coupled. For the efficient implementation on velocity level, adaptations are necessary which may result in the loss of the interpretation as time-discontinuous Galerkin method. The trapezoidal rule as a locally second order scheme, however, suffices for most practical considerations and industrial simulations.

6 Multi-contact examples

In this section, we discuss several examples to show the benefits of the proposed scheme. The slider-crank mechanism is a nonlinear example and the bouncing ball in a box is a linear example. We compare computational results, convergence and computing time of the half-explicit timestepping schemes on acceleration and velocity level, as well as of the classic explicit Moreau-Jean timestepping scheme. The computations have been done with Matlab. Thereby index sets are calculated without any additional tolerances. The constraints are calculated with a tolerance of 10^{-12} for satisfying the constraint equations.

6.1 Slider-crank mechanism

For the slider-crank mechanism in Sect. 2.1, we give some supplementary impressions without regarding friction. The calculations have been performed with the half-explicit timestepping scheme on velocity level. Figure 11 shows the slider's movement in the notch for different coefficients of restitution. In Fig. 12, the trajectories of the three generalized coordinates and generalized velocities are depicted, respectively. Figure 13 demonstrates nicely the splitting of the different Lagrange multipliers and therefore the possibility to achieve locally a higher order discretization.

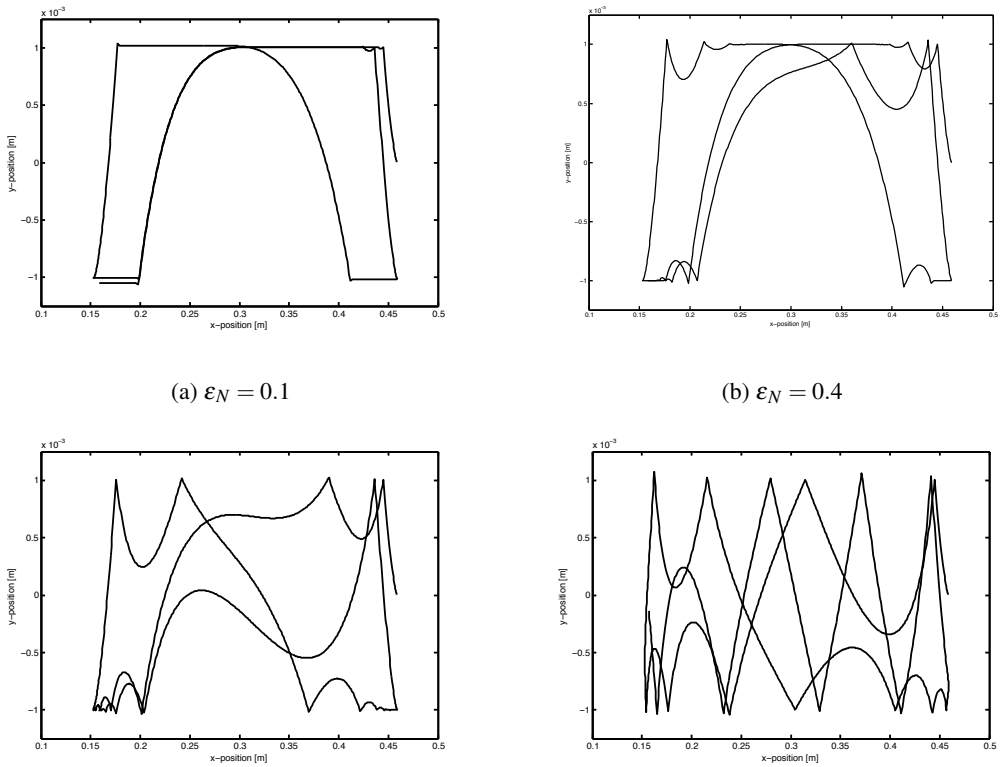

(a) $\varepsilon_N = 0.1$ (b) $\varepsilon_N = 0.4$

(c) $\varepsilon_N = 0.6$ (d) $\varepsilon_N = 0.9$

Figure 11: Movement of the center of gravity of the slider for different coefficients of restitution and half-explicit timestepping on velocity level.

6.1.1 Convergence and computing time for the bilateral case

We compare the half-explicit timestepping scheme on velocity level with the classic explicit Moreau-Jean timestepping scheme regarding a bilateral slider-crank mechanism without friction, i.e., $c = 0\,\mathrm{m}$. Thereby, we analyze computing time and convergence of the schemes in comparison with a corresponding Simpack model, which is integrated with the SODASRT2 solver and a high tolerance 10^{-12}.

Independent of different time step-sizes, the relative overhead of the half-explicit timestepping scheme on velocity level in comparison with the classic explicit Moreau-Jean timestepping scheme is about 1.2. Hence, the computation time per time step is about 1.2 times larger for the half-explicit timestepping scheme on velocity level. We calculate the error with respect to the reference Simpack solution for different time step-sizes. Thereby, we compute the differences of the generalized coordinates for the considered time instances and arrange them in a matrix. The 2-norm of this matrix results in Table 2. Concerning these evaluations, this is a trend to an order of convergence of 1 for the classic explicit Moreau-Jean timestepping scheme and to an order of convergence of 2 for the half-explicit timestepping scheme on velocity level. The overall relative cost to achieve a given tolerance, e.g. 10^{-2}, is given by the relation of the fractions of the relative overhead and the necessary time step-size, i.e., $1.2 \cdot 10^{-1}$ for the half-explicit timestepping scheme on velocity level in comparison to the classic explicit Moreau-Jean timestepping scheme. Thus, it makes sense to apply higher-order approximations for appropriate

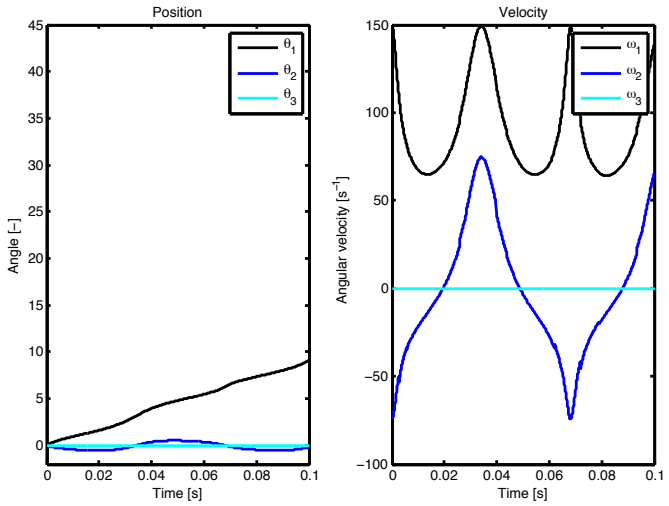

Figure 12: Angles and angular velocities of the slider-crank mechanism for half-explicit timestepping on velocity level.

Δt [s]	10^{-3}	10^{-4}	10^{-5}
error of the classic explicit Moreau-Jean timestepping scheme	$6.9 \cdot 10^{-1}$	$2.1 \cdot 10^{-1}$	$6.6 \cdot 10^{-2}$
error of the half-explicit timestepping scheme on velocity level	$4.2 \cdot 10^{-1}$	$2.4 \cdot 10^{-2}$	$8.4 \cdot 10^{-4}$

Table 2: Bilateral slider-crank example: comparison of the error for different time step-sizes.

examples.

6.1.2 Convergence and computing time for the unilateral case

We compare the half-explicit timestepping scheme on velocity level with the classic explicit Moreau-Jean timestepping regarding a unilateral slider-crank mechanism with friction. Thereby, we analyze computing time and convergence of the schemes assuming a reference solution given by a simulation of the half-explicit timestepping on velocity level with $\Delta t = 10^{-7}$ s.

The relative overhead of the half-explicit timestepping scheme on velocity level is about 1.15. For the error, we get Table 3. The order of convergence concerning these evaluations drops down to 1 for both

Δt [s]	10^{-3}	10^{-4}	10^{-5}
error of the classic explicit Moreau-Jean timestepping scheme	$7.1 \cdot 10^{-1}$	$1.5 \cdot 10^{-1}$	$4.5 \cdot 10^{-2}$
error of the half-explicit timestepping scheme on velocity level	$4.7 \cdot 10^{-1}$	$1.8 \cdot 10^{-2}$	$3.3 \cdot 10^{-3}$

Table 3: Unilateral slider-crank example: comparison of the error for different time step-sizes.

integration schemes. However, the results for the half-explicit timestepping scheme on velocity level are better perhaps because of the possibility to achieve a locally higher order. The overall relative cost for

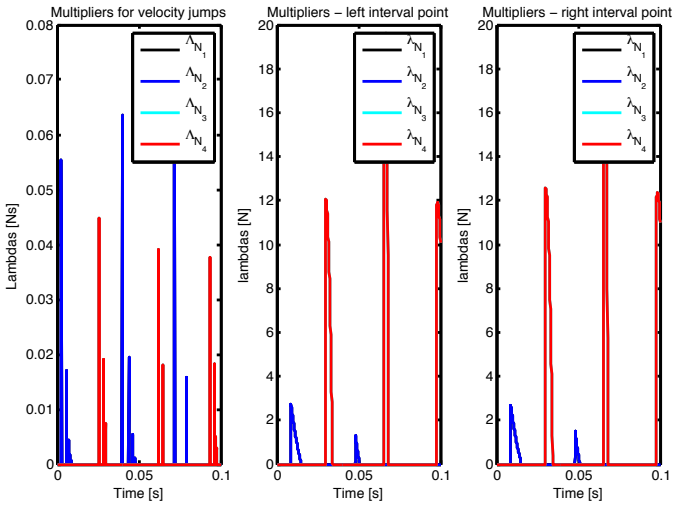

Figure 13: Lagrange multipliers of the slider-crank mechanism for half-explicit timestepping on velocity level.

a given tolerance, e.g. 10^{-2}, is $1.15 \cdot 10^{-1}$ for the half-explicit timestepping scheme on velocity level in comparison to the classic explicit Moreau-Jean timestepping scheme. Hence like in the bilateral case, the relative overhead could be compensated by an adaptive time-step size and a control of the accuracy.

6.2 Bouncing ball in a box

The linear bouncing ball in a box example explains the difference between the half-explicit timestepping schemes on acceleration and velocity level, i.e., the drift-off effect, and the energy behavior of half-explicit timestepping schemes based on the trapezoidal rule.

A bouncing ball of radius R in a planar box of width a and height b (Fig. 14) is described by the two translational coordinates, x and y, of its center of gravity. The rigid ball with mass m is subject to gravitation γ in $-\begin{pmatrix}\cos(\pi/6) & \sin(\pi/6)\end{pmatrix}^T$-direction. The normal gap functions g_N are shown in Fig. 14. The vector containing the coefficients of restitution is ε_N. Friction is not considered. Fixed characteristics are given in Table 4.

The generalized mass matrix satisfies

$$M : \mathbb{R}^2 \to \mathbb{R}^{2,2}\ ,\ q \mapsto M(q) = \begin{pmatrix} \mathrm{m} & 0 \\ 0 & m \end{pmatrix}\ , \tag{132}$$

and the linear generalized force can be obtained by

$$h : \mathbb{R}^2 \times \mathbb{R}^2 \to \mathbb{R}^2\ ,\ (q,v) \mapsto h(q,v) = \gamma \begin{pmatrix} \cos(\pi/6) \\ \sin(\pi/6) \end{pmatrix}\ . \tag{133}$$

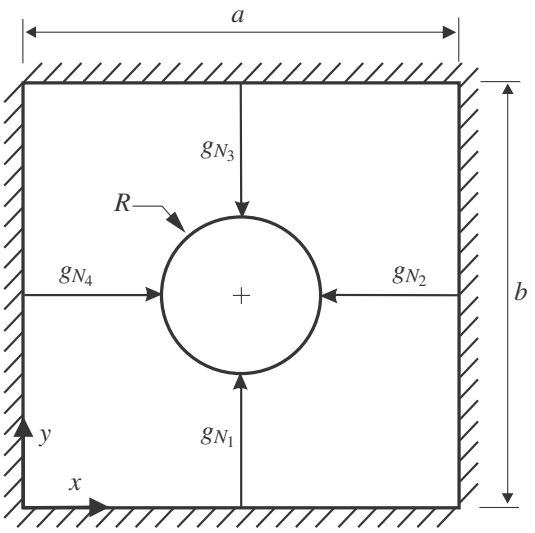

Figure 14: Bouncing ball in a box.

Geometrical characteristics	$a = 4.0\,\mathrm{m}$
	$b = 4.0\,\mathrm{m}$
	$R = 1.0\,\mathrm{m}$
Inertia properties	$m = 1.0\,\mathrm{kg}$
Force elements	$\gamma = 9.81\,\mathrm{m/s^2}$
Contact parameters	$\varepsilon_{N_1} = \varepsilon_{N_2} = \varepsilon_{N_3} = \varepsilon_{N_4} = 0.3$
Initial conditions	$x_0 = 2.0\,\mathrm{m}$
	$y_0 = 2.0\,\mathrm{m}$
	$\dot{x}_0 = 0.0\,\mathrm{m/s}$
	$\dot{y}_0 = 0.0\,\mathrm{m/s}$

Table 4: Characteristics of the bouncing ball example.

The normal gap functions are

$$g_{N_1}(q) = y - R\,, \tag{134}$$
$$g_{N_2}(q) = a - x - R\,, \tag{135}$$
$$g_{N_3}(q) = b - y - R\,, \tag{136}$$
$$g_{N_4}(q) = x - R\,, \tag{137}$$

resulting in a Boolean matrix for the generalized force directions.

Fig. 15 shows the trajectory of the ball starting from its initial position and ending in the lower left corner. The position and velocity curves are depicted in Fig. 16 and clearly show the nonsmooth, i.e., impulsive behavior. For the application of the half-explicit timestepping methods based on the trapezoidal rule to the slider-crank mechanism, we have mentioned a not always decreasing energy trend (Fig. 6). As we see in Fig. 17, the energy behavior for the linear bouncing ball in a box example actually shows the expected curve without any increasing periods. The previous non-decreasing trend is traced back to the nonlinear nature of the example. In Fig. 18, we can convince ourselves from the drift-off effect for the acceleration level discretization. We have to remark, that the half-explicit timestepping on acceleration

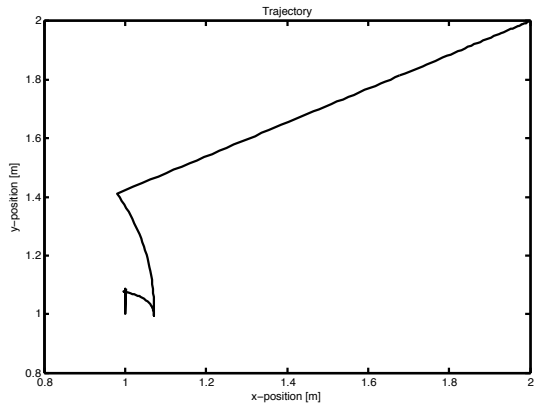

Figure 15: Trajectory of the bouncing ball in a box for half-explicit timestepping on velocity level.

level just *evaluates* the contact forces similar to the explicit timestepping on velocity level. This procedure is more a calculation of equivalent forces involving a projection than a computation of contact forces while adapting the unknowns of the system. That is why, we see the drift-off effect also for the linear bouncing ball in a box example. All calculations have been performed with $\Delta t = 5 \cdot 10^{-3}\,\mathrm{s}$.

7 Flexible examples

The elastic bar is a linear but flexible example and the rotor is a linear and flexible example from practice. In this section, we discuss the behavior of waves and damping for half-explicit timestepping schemes on velocity level.

7.1 Elastic bar

In this section, we consider the classical example of a linear elastic bar that impacts a rigid obstacle at constant velocity v_0. The example is depicted in Figure 19. The bar has a length L, a section area S, a density ρ and a Young modulus E. If we denote by $c_0 = \sqrt{E/\rho}$ the longitudinal wave speed, the time of contact is twice the time of the traveling of elastic waves in the bar, that is $T = 2L/c_0$. Within the contact time, the contact force is constant and equals $\tau = ESv_0/c_0$. The parameters for this example are summarized in Table 5. The bar is discretized by N linear rod finite elements. The elementary mass and

Geometrical characteristics	$L = 1\,\mathrm{m}$
	$S = \pi \cdot 10^{-4}\,\mathrm{m}^2$
Material properties	$\rho = 7800\,\mathrm{kg/m}^3$
	$E = 2.1 \cdot 10^{1}\,\mathrm{N/m}^2$
Initial conditions	$v_0 = 0.1\,\mathrm{m/s}$
Solution characteristics	$c_0 = 5.188 \cdot 10^{3}\,\mathrm{m/s}$
	$T = 3.854 \cdot 10^{-4}\,\mathrm{s}$
	$\tau = 1.271 \cdot 10^{3}\,\mathrm{N}$

Table 5: Characteristics of the elastic bar example.

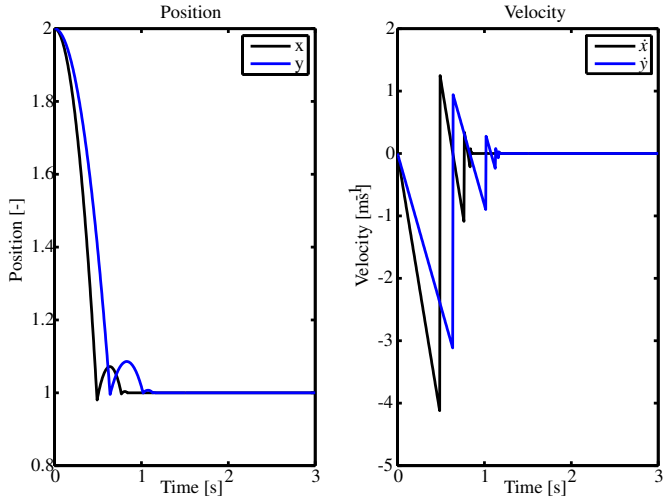

Figure 16: Position and velocity of the bouncing ball in a box for half-explicit timestepping on velocity level.

stiffness matrices are

$$M_e = \frac{1}{6}\rho S l_e \begin{bmatrix} 2 & 1 \\ 1 & 2 \end{bmatrix}, \quad K_e = \frac{1}{l_e} ES \begin{bmatrix} 1 & -1 \\ -1 & 1 \end{bmatrix}, \tag{138}$$

where $l_e = L/N$ is the length of an element. The first simulation results with the half-explicit timestepping scheme on velocity level for a time-step size $\Delta t = 10^{-7}$ s and 50 finite elements are reported in Fig. 20. This simulation has been carried out with Siconos, an open-source software for the modelling and the simulation of nonsmooth dynamical systems [4]. In this simulation, the expected solution for the elastic bar is found exaclty with Lemke's algorithm. The time of contact of the bar is well-approximated and the velocity within the contact interval is maintained at zero. The violation of the constraint is equal to $5 \cdot 10^{-9}$ m. The presence of the impulse is a consequence of the space discretization by finite elements. The finite mass of the node in contact is instantaneously stopped at the impact. This generates an impulse. This impulse associated with a plastic impact induces a loss of the total energy at impact which can be observed in the energy plot. Finally, we remark that the reaction force is well approximated in the first half of the contact period before the development of an instability which is inherent to standard finite element approximations of a travelling velocity jump trough the mesh. Nevertheless, it is noteworthy that the contact is never lost due to artificial numerical chattering.

In Figure 21, a similar simulation is reported but the number of elements is increased to 1000. We observe that the reaction impulse is reduced due to the decreased mass of the node in contact. The energy loss is also reduced. The instability is nevertheless still visible but its frequency has increased with the inverse of the element size. The travelling of the impulse excites the spurious high frequency mode associated with the discretization. One of the usual ways to circumvent this problem is to introduce an artificial damping in the simulation. Since the discretization family presented in this paper does not include numerical damping- even if it seems possible, it is left as further work-, we have added a small amount of Rayleigh damping (proportional to the stiffness $C_e = \delta K_e$) to damp out this numerical artifact. In Figure 22, the results with the viscous damping are plotted. The stiffness proportional damping coefficient is equal to $\delta = 10^{-3}/E\,\mathrm{s} = 4.761 \cdot 10^{-6}\,\mathrm{s}$. We observe that the instability is nearly damped out and the post velocity is smooth. Only a remaining impulse travels trough the bar. The decay of the total energy can be

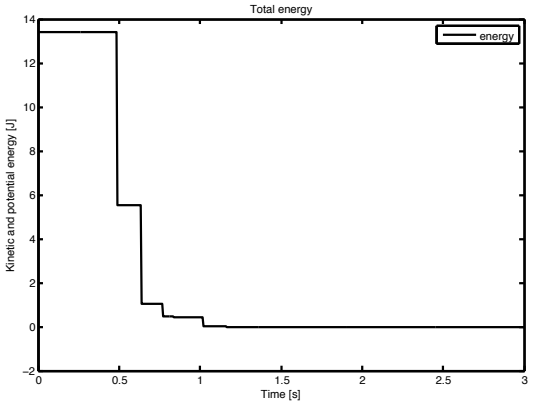

Figure 17: Total energy of the bouncing ball in a box for half-explicit timestepping on velocity level.

seen in the energy plot.

If we compare our results with those in [1] for the standard Moreau-Jean timestepping scheme for the example of the elastic bar, we observe the same type of instability of the reaction forces when there is no numerical damping in the Moreau-Jean algorithm. Nevertheless, the proposed scheme is mainly interesting for two reasons. First, it enables a splitting between the reaction force and the artificial reaction impulse due to the space discretization. The value of the reaction force and the stress in the bar can be used for design as a good approximation of the forces in the space continuous bar. The magnitude of the reaction impulse gives a measure of the quality of the mesh with respect to the contact representation. Second, the scheme is half-explicit and thus requires less computational effort for the evaluation of the constitutive behavior in the nonlinear setting. However, we have to notice that a CFL type condition has to be satisfied since the internal forces are explicitly evaluated.

7.2 Rotor

A rotor test rig at the Institute of Applied Mechanics of the Technische Universität München is modelled in the multibody simulation framework MBSim [mbsim, 52] (Fig. 23). The idea of this example is the implementation of a variant of the half-explicit timestepping scheme on velocity level in MBSim and the application to an industrial example. Thereby, we test a simple and heuristic adaptation of the time-step size.

The rotor in Fig. 23 consists of drive system with a driving torque about the rotor's longitudinal axis T_D and a failure given by a torque about the vertical axis T_F. The drive system is mounted by a spring-damper element with constants c_D, d_D. The rotor's axle is modelled with N_A beam elements in a floating frame of reference framework. Each finite element node has five degrees of freedom, two small out-off plane translational deflections, two small out-off plane rotational deflections and the rotation about the rotor's longitudinal axis. The length of the axle is l_A, its radius is r_A, the density is ρ_A, the Young's modulus is E_A, and the shear modulus is G_A. A mass proportional damping d_{1_A} and a torsional damping d_{2_A} are used. The fly-wheel is a rigid body with originally six degrees of freedom, which is mounted bilaterally at position x_F from the axle's left end on the rotor's axle. It has the mass m_F and the rotational inertia about the rotor's longitudinal axis J_F. The journal bearing consists of a rigid frustum with six degrees of freedom mounted bilaterally in its center on the left end of the rotor's axle but with negligible inertia values. This frustum of radius r_{JF} and half width b_{JF} moves freely in a circular bearing with

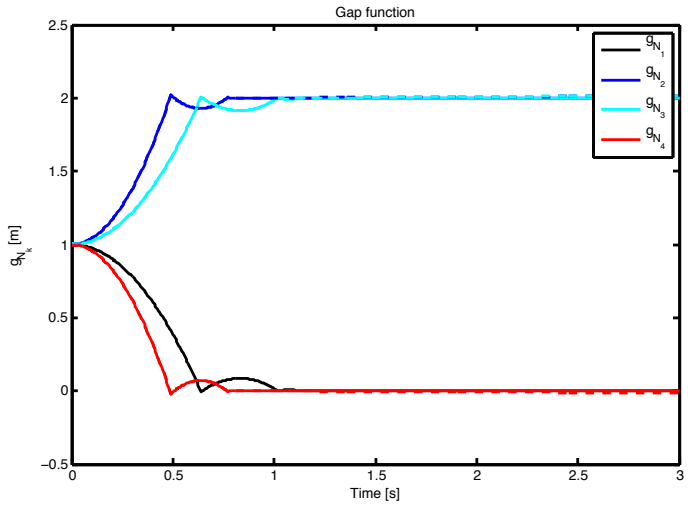

Figure 18: Normal gap functions of the bouncing ball in a box for half-explicit timestepping on acceleration (dotted) and velocity level (solid).

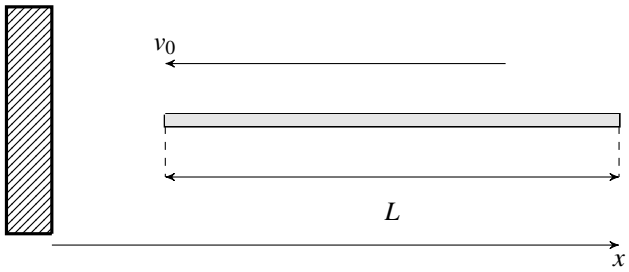

Figure 19: Linear elastic impacting bar on a rigid obstacle.

radius r_{JB}, i.e., backlash and dry friction μ. The bearing is a rigid body with six degrees of freedom, mass m_{JB} and negligible rotational inertia values. The bearing is mounted in its center by a spring-damper element with constants c_{JB}, d_{JB}. The actual contact may only occur at position x_{JB} from the axle's left end. We consider the bearing, e.g., as an auxiliary bearing occurring in many rotor systems with active magnetic bearings [26] or as an example for a safety bearing. The whole system is subject to gravitation γ in negative vertical direction. The characteristics are summarized in Table 6. Damping is added because of the experience in Sect. 7.1.

For an implementation of a variant of the half-explicit timestepping scheme on velocity level in MBSim, especially we have to discretize

$$\dot{q} = Y(q)v \tag{139}$$

instead of $\dot{q} = v$ in the sense of [9]. At the same time, we adapt the interpretation of the contact activity

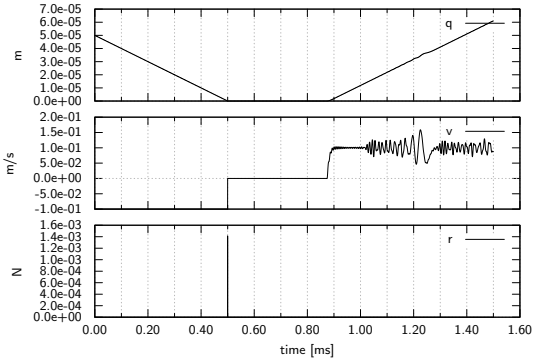

(a) position, velocity and reaction at the contact point

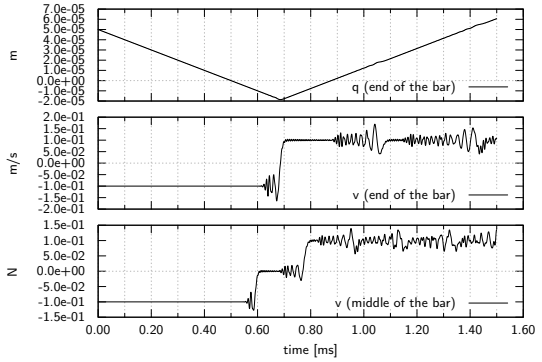

(b) position, velocity and reaction at the tip

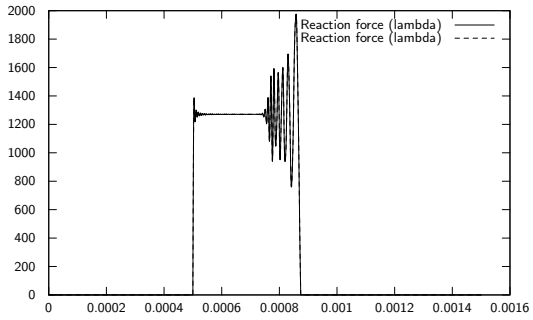

(c) reaction forces λ

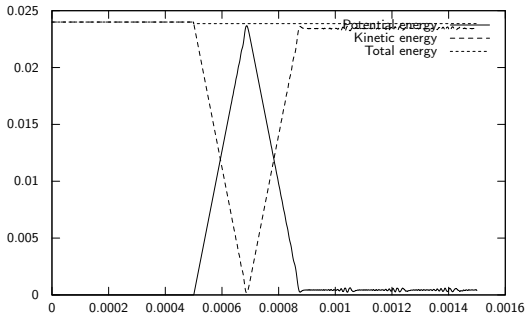

(d) kinetic, potential and total energy

Figure 20: Elastic bar simulation with the half-explicit timestepping scheme on velocity level $\Delta t = 1 \cdot 10^{-7}$ s, $N = 50$.

for the first stage unknowns. Instead of (123)-(124), we solve

$$0 = \lambda^{+}_{N_{i-1},\mathscr{I}_1^{i-1,1}} - \mathrm{proj}_{\mathbb{R}_0^+}\left(\lambda^{+}_{N_{i-1},\mathscr{I}_1^{i-1,1}} - rW^{T}_{N,\mathscr{I}_1^{i-1,1}}(q_{i-1,1})v_{i-1,1}\right), \tag{140}$$

$$0 = \lambda^{+}_{T_{i-1},\mathscr{I}_1^{i-1,1}} - \mathrm{proj}_{C_T(\lambda^{+}_{N_{i-1},\mathscr{I}_1^{i-1,1}})}\left(\lambda^{+}_{T_{i-1},\mathscr{I}_1^{i-1,1}} - rW^{T}_{T,\mathscr{I}_1^{i-1,1}}(q_{i-1,1})v_{i-1,1}\right) \tag{141}$$

in a more natural way. An overview is depicted in Fig. 24. The time-step size for impulsive periods $\tilde{\Delta t}$ is heuristically adapted concerning the experiences with the slider-crank example (Table 3): $\tilde{\Delta t} = \frac{\Delta t}{10}$. As we do not know the error constant, we prefer this heuristic in comparison to $\tilde{\Delta t} = \Delta t^2$, which uses the non-impulsive order of the schemes.

The typical forward whirl phenomenon because of the external loadings and the dry friction contact can be seen in Fig. 25. We are interested in the general behavior of the variant of the half-explicit timestepping scheme on velocity level. In MBSim, the tolerances define tubes around the corner laws [23]. Starting from the impulsive tolerances $tol_\Lambda = 10^{-10}$ Ns, $tol_{\dot g} = 10^{-10}$ m/s, we use $tol_\lambda = \frac{tol_\Lambda}{\Delta t}$, $tol_{\ddot g} = \frac{tol_{\dot g}}{\Delta t}$ for the calculation of the constraint equations with a single-step fixed-point method [23]. The index sets are detected with a tolerance of 10^{-8} m. The variant of the half-explicit timestepping scheme on velocity level uses a fraction of impulsive integration steps of 1.3%. The overall computing time of the variant of the half-explicit timestepping scheme on velocity level in comparison with the half-explicit variant of the Moreau-Jean timestepping scheme in [mbsim] is 0.32. Hence, the new proposed scheme offers huge

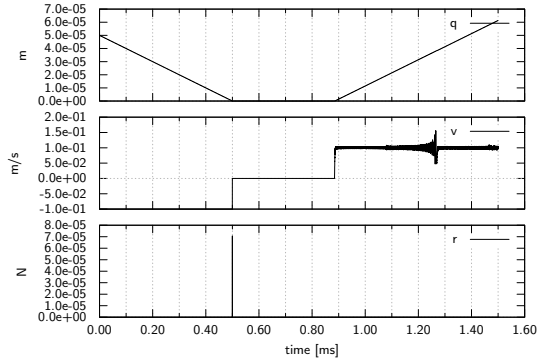

(a) position, velocity and reaction impulse at the contact point

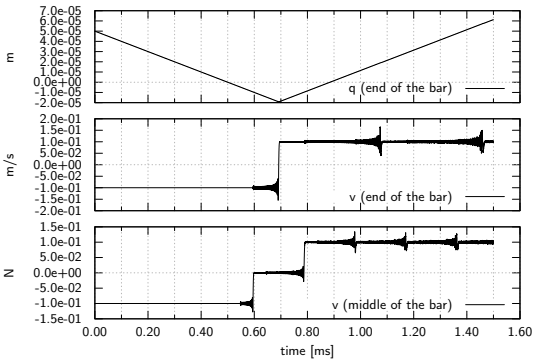

(b) position, velocity and reaction at the tip

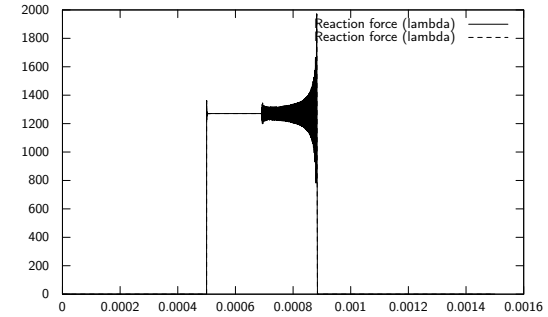

(c) reaction forces λ

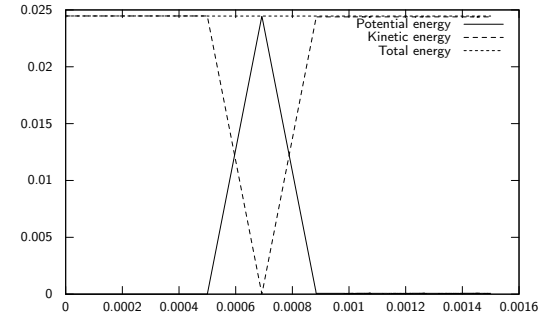

(d) kinetic, potential and total energy

Figure 21: Elastic bar simulation with the half-explicit timestepping scheme on velocity level $\Delta t = 1 \cdot 10^{-7}$ s, $N = 1000$.

computing time saving potential. In the calculations, we have used $\Delta t = 5 \cdot 10^{-6}$ s.

8 Summary and Conclusion

We have presented a time-discretization scheme for the simulation of nonsmooth mechanical systems with friction and impacts as well as rigid and flexible bodies with all possible interactions. Without switching between impulsive and non-impulsive periods, the time-discretization scheme is both consistent and efficient. It represents impulses, if necessary, and automatic local order elevation for state variables, if possible, at the same time and is unique in the literature concerning these criteria. Constraints are formulated on velocity level in an implicit way using an augmented Lagrangian technique with semi-smooth Newton schemes without penetration; all other evaluations are explicit, which yields a half-explicit method. The scheme is derived and explained in detail concerning different criteria and it is applied to various examples with multi-contact, flexibility and industrial relevance. As a compromise between classic timestepping schemes and event-driven integration in the context of time-discontinuous Galerkin methods finally, two half-explicit timestepping schemes on velocity level distinguish impulsive and non-impulsive periods for all examples in a geometrically consistent way and reduce the computing time significantly. For flexible examples, we recognize the drawback of explicit schemes, i.e., stability issues, which can be solved by applying schemes from the Newmark family as base integration schemes

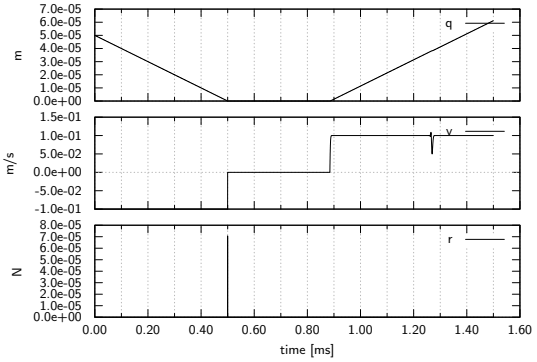

(a) position, velocity and reaction impulse at the contact point

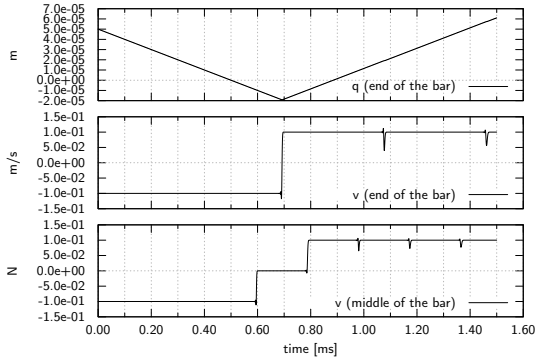

(b) position, velocity and reaction at the tip

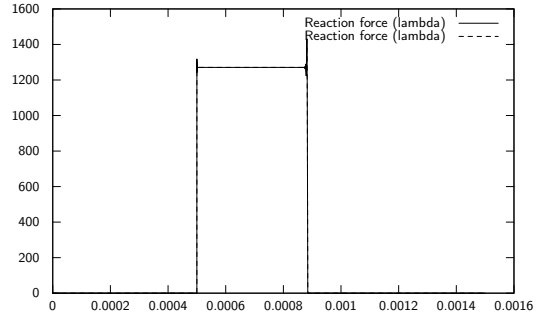

(c) reaction forces λ

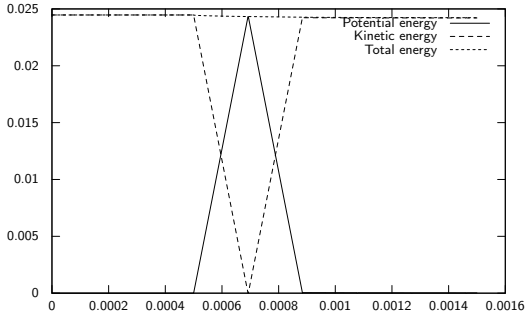

(d) kinetic, potential and total energy

Figure 22: Damped elastic bar simulation with the half-explicit timestepping scheme on velocity level $\Delta t = 1 \cdot 10^{-7}$ s, $N = 1000$.

in the framework of foreseen velocity jumps and respective impulses at the end of each discretization interval. This is left for future work.

Acknowledgement

JK gratefully acknowledges the UK's Engineering and Physical Sciences Research Council (EPSRC) for funding through a studentship.

References

[1] Vincent Acary. Projected event-capturing time-stepping schemes for nonsmooth mechanical systems with unilateral contact and Coulomb's friction. *Comput Methods Appl Mech Engrg*, 256: 224–250, 2013. ISSN 0045-7825.

[2] Vincent Acary. Higher order event capturing time-stepping schemes for nonsmooth multibody systems with unilateral constraints and impacts. *Appl Numer Math*, to appear 2011. ISSN 0168-9274.

[3] Vincent Acary and Bernard Brogliato. *Numerical methods for nonsmooth dynamical systems :*

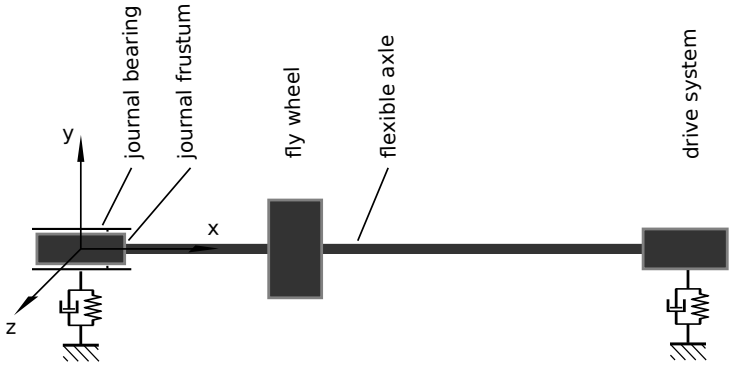

Figure 23: Model of a rotor test rig.

applications in mechanics and electronics, volume 35 of *Lecture notes in applied and computational mechanics*. Springer, Berlin, 1st edition edition, 2008. ISBN 3-540-75391-5.

[4] Vincent Acary and Franck Perignon. An introduction to Siconos. Technical report, INRIA, 2007. URL `http://siconos.gforge.inria.fr`.

[5] Pierre Alart and Alain Curnier. A mixed formulation for frictional contact problems prone to Newton like solution methods. *Comput Methods Appl Mech Engrg*, 92:353 – 375, 1991. ISSN 0045-7825.

[6] Martin Arnold. Numerical methods for simulation in applied dynamics. In Martin Arnold and Werner Schiehlen, editors, *Simulation Techniques for Applied Dynamics*, number 507 in CISM International Centre for Mechanical Sciences, pages 191–246. Springer, Wien, 2009. ISBN 978-3-211-89548-1.

[7] Martin Arnold and Ander Murua. Non-stiff integrators for differential algebraic systems of index 2. *Numerical Algorithms*, 19(1-4):25–41, 1998. ISSN 1017-1398.

[8] Olivier Bauchau. *Flexible Multibody Dynamics*. Springer, Berlin, 2010. ISBN 978-9-400-70335-3.

[9] Valerie Brasey. Hem 5 user's guide. Technical report, Universite de Geneve, Suisse, 1994.

[10] Valerie Brasey. *Methodes demi-explicites pour equations differentielles algebraiques semi-explicites d'index 2*. PhD thesis, Universite de Geneve, 1994.

[11] Bernard Brogliato. *Nonsmooth mechanics : models, dynamics and control*. Communications and control engineering. Springer, London, 2nd edition edition, 1999. ISBN 1-85233-143-7.

[12] Olivier Brüls, Vincent Acary, and Alberto Cardona. Simultaneous enforcement of constraints at position and velocity levels in the nonsmooth generalized-α scheme. *Computer Methods in Applied Mechanics and Engineering*, 281:131–161, November 2014. ISSN 0045-7825. doi: 10.1016/j.cma.2014.07.025. URL `http://hal.inria.fr/hal-01059823`.

[13] Qiong-Zhong Chen, Vincent Acary, Geoffrey Virlez, and Olivier Brüls. A nonsmooth generalized-α scheme for flexible multibody systems with unilateral constraints. *Int J Numer Meth Eng*, 2013. ISSN 0029-5981.

[14] P.W. Christensen, Anders Klarbring, Jong-Shi Pang, and Niclas Strömberg. Formulation and comparison of algorithms for frictional contact problems. *Int J Numer Meth Eng*, 42(1):145–173, 1998. ISSN 1097-0207.

rotor axle	$l_A = 0.59\,\mathrm{m}$
	$r_A = 12.5 \cdot 10^{-3}\,\mathrm{m}$
	$\rho_A = 7.85 \cdot 10^{3}\,\mathrm{kg/m^3}$
	$E_A = 2.1 \cdot 10^{11}\,\mathrm{N/m^2}$
	$G_A = 0.81 \cdot 10^{11}\,\mathrm{N/m^2}$
	$d_{1_A} = 60\,1/\mathrm{s}$
	$d_{2_A} = 0.001\,\mathrm{kgm^2/s}$
fly wheel	$m_F = 4.98\,\mathrm{kg}$
	$J_F = 0.01\,\mathrm{kgm^2}$
	$x_F = 1.8 \cdot 10^{-1}\,\mathrm{m}$
journal frustum	$r_{JF} = 10^{-2}\,\mathrm{m}$
	$b_{JF} = 19 \cdot 10^{-3}\,\mathrm{m}$
journal bearing	$r_{JB} = 1.01 \cdot 10^{-2}\,\mathrm{m}$
	$m_{JB} = 2.3\,\mathrm{kg}$
	$x_{JB} = b_{JF}/2$
	$\mu = 0.01$
	$c_{JB} = 10^{6}\,\mathrm{N/m}$
	$d_{JB} = 10\,\mathrm{Ns/m}$
drive system	$T_D = 100\,\mathrm{Nm}$ for $0.05\,\mathrm{s}$
	$T_F = 10\,\mathrm{Nm}$
	$c_F = 6 \cdot 10^{6}\,\mathrm{N/m}$
	$d_F = 10\,\mathrm{Ns/m}$
gravitation	$\gamma = 9.81\,\mathrm{m/s^2}$

Table 6: Characteristics of the rotor example.

[15] Jintai Chung and Gregory Hulbert. A time integration algorithm for structural dynamics with improved numerical dissipation: the generalized-α method. *J Appl Mech*, 60:371–375, 1993. ISSN 0021-8936.

[16] Peter Deuflhard and Folkmar Bornemann. *Scientific computing with ordinary differential equations*, volume 42 of *Texts in applied mathematics*. Springer, New York, 2002. ISBN 0-387-95462-7.

[17] Peter Deuflhard, Rolf Krause, and Susanne Ertel. A contact-stabilized newmark method for dynamical contact problems. *Int J Numer Meth Eng*, 73(9):1274–1290, 2008. ISSN 1097-0207.

[18] David Doyen, Alexandre Ern, and Serge Piperno. Time-integration schemes for the finite element dynamic Signorini problem. *SIAM J Sci Comput*, 33:223–249, 2011. ISSN 1064-8275.

[19] Edda Eich-Soellner and Claus Führer. *Numerical methods in multibody dynamics*. European Consortium for Mathematics in Industry. Teubner, Stuttgart, 2nd corr. reprint 2008 edition, 1998. ISBN 3-519-02601-5.

[20] Bastian Esefeld, Thorsten Schindler, and Heinz Ulbrich. A coupling approach for the numerical integration of non-smooth multibody systems. In *Proceedings of the 4th Canadian Conference on Nonlinear Solid Mechanics, McGill University Montreal, Canada, 23rd-26th July 2013*, 2013.

[21] Razvan Fetecau, Jerrold Marsden, Michael Ortiz, and Matthew West. Nonsmooth lagrangian mechanics and variational collision integrators. *SIAM J Appl Dyn Syst*, 2:381–416, 2003. ISSN 1536-0040.

Specify characteristics, start time $t = 0$, end time T, time step size Δt

Initialize $i = 1$
For $t < T$
Evaluate left-hand side
Evaluate $q_{i-1,0} = q_{i-1}$
Evaluate $v_{i-1,0} = v_{i-1}^+$

Predict right-hand side
Compute $q_{i-1,1} = q_{i-1,0} + \Delta t_i Y_{i-1,0} v_{i-1,0}$

Decide strategy
if $\nexists k^* : g_{N_{k^*}}(q_{i-1,0}) > 0 \wedge g_{N_{k^*}}(q_{i-1,1}) \le 0$
Set $\Lambda_{N_i} = 0$, $\Lambda_{T_i} = 0$
Compute Lagrange multipliers on velocity level

$$\lambda^+_{N_{i-1},\mathscr{I}_1^{i-1,1}} - \mathrm{proj}_{\mathbb{R}_0^+}\left(\lambda^+_{N_{i-1},\mathscr{I}_1^{i-1,1}} - rW^T_{N_{i-1,1},\mathscr{I}_1^{i-1,1}} v_{i-1,1}\right) = 0$$

$$\lambda^+_{T_{i-1},\mathscr{I}_1^{i-1,1}} - \mathrm{proj}_{C_T(\lambda^+_{N_{i-1},\mathscr{I}_1^{i-1,1}})}\left(\lambda^+_{T_{i-1},\mathscr{I}_1^{i-1,1}} - rW^T_{T_{i-1,1},\mathscr{I}_1^{i-1,1}} v_{i-1,1}\right) = 0$$

with $v_{i-1,1} = v_{i-1,0} + \Delta t_i M^{-1}_{i-1,0}\left[h_{i-1,0} + W_{N_{i-1,0}}\lambda^+_{N_{i-1}} + W_{T_{i-1,0}}\lambda^+_{T_{i-1}}\right]$

Compute $q_i = q_{i-1,0} + \frac{\Delta t_i}{2}\left\{Y_{i-1,0}v_{i-1,0} + Y_{i-1,1}v_{i-1,1}\right\}$
Compute Lagrange multipliers on velocity level

$$\lambda^-_{N_i,\mathscr{I}_1^i} - \mathrm{proj}_{\mathbb{R}_0^+}\left(\lambda^-_{N_i,\mathscr{I}_1^i} - rW^T_{N_i,\mathscr{I}_1^i} v_i^-\right) = 0$$

$$\lambda^-_{T_i,\mathscr{I}_1^i} - \mathrm{proj}_{C_T(\lambda^-_{N_i,\mathscr{I}_1^i})}\left(\lambda^-_{T_i,\mathscr{I}_1^i} - rW^T_{T_i,\mathscr{I}_1^i} v_i^-\right) = 0$$

with $v_i^+ = v_i^- = v_{i-1,0} + \frac{\Delta t_i}{2} M^{-1}_{i-1,0}\left[h_{i-1,0} + W_{N_{i-1,0}}\lambda^+_{N_{i-1}} + W_{T_{i-1,0}}\lambda^+_{T_{i-1}}\right] + \frac{\Delta t_i}{2} M_i^{-1}\left[h(q_i, v_{i-1,1}) + W_{N_i}\lambda^-_{N_i} + W_{T_i}\lambda^-_{T_i}\right]$

if $\exists k^* : g_{N_{k^*}}(q_{i-1,0}) > 0 \wedge g_{N_{k^*}}(q_{i-1,1}) \le 0$
Set $\lambda^+_{N_{i-1}} = 0$, $\lambda^+_{T_{i-1}} = 0$ and $\lambda^-_{N_i} = 0$, $\lambda^-_{T_i} = 0$
Compute $q_{i-1,1} = q_{i-1,0} + \tilde{\Delta} t_i Y_{i-1,0} v_{i-1,0}$
Compute $v_{i-1,1} = v_{i-1,0} + \tilde{\Delta} t_i M^{-1}_{i-1,0} h_{i-1,0}$
Compute $q_i = q_{i-1,0} + \frac{\tilde{\Delta} t_i}{2}\left\{Y_{i-1,0}v_{i-1,0} + Y_{i-1,1}v_{i-1,1}\right\}$
Compute $v_i^- = v_{i-1,0} + \frac{\tilde{\Delta} t_i}{2}\left\{M^{-1}_{i-1,0}h_{i-1,0} + M_i^{-1}h(q_i, v_{i-1,1})\right\}$
Compute Lagrange multipliers on velocity level

$$\Lambda_{N_i,\mathscr{I}_1^i} - \mathrm{proj}_{\mathbb{R}_0^+}\left[\Lambda_{N_i} - r\dot{\tilde{g}}_{N_i,\mathscr{I}_1^i}\right] = 0$$

$$\Lambda_{T_i,\mathscr{I}_1^i} - \mathrm{proj}_{C_T(\Lambda_{N_i})}\left[\Lambda_{T_i} - r\dot{\tilde{g}}_{T_i,\mathscr{I}_1^i}\right] = 0$$

with $v_i^+ = v_i^- + M_i^{-1}(W_{N_i}\Lambda_{N_i} + W_{T_i}\Lambda_{T_i})$

Write result of time step, e.g. q_i and v_i^+

Update t by Δt_i respectively $\tilde{\Delta} t_i$ and increment i by 1

Postprocessing

Figure 24: Flowchart of the half-explicit timestepping scheme on velocity level, variant for MBSim.

[22] Paulo Flores, Remco Leine, and Christoph Glocker. Modeling and analysis of planar rigid multibody systems with translational clearance joints based on the non-smooth dynamics approach. *Multibody*

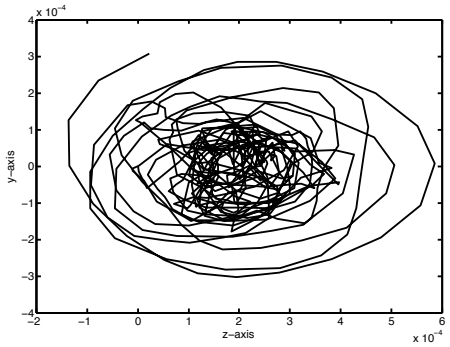

Figure 25: Curve of the journal frustum in the journal bearing.

System Dynamics, 23:165–190, 2010. ISSN 1573-272X.

[23] Martin Förg. *Mehrkörpersysteme mit mengenwertigen Kraftgesetzen : Theorie und Numerik*, volume 411 of *Fortschritt-Berichte VDI : Reihe 20, Rechnerunterstützte Verfahren*. VDI Verlag, Düsseldorf, als Manuskript gedruckt edition, 2007. ISBN 978-3-18-341120-7.

[24] Claus Führer and Ben Leimkuhler. Numerical solution of differential-algebraic equations for constrained mechanical motion. *Numer Math*, 59:55–69, 1991. ISSN 0029-599X.

[25] Charles William Gear, Ben Leimkuhler, and G.K. Gupta. Automatic integration of Euler-Lagrange equations with constraints. *J Comput Appl Math*, pages 77–90, 1985. ISSN 0377-0427.

[26] Lucas Ginzinger, Mehmet Sahinkaya, Thorsten Schindler, Heinz Ulbrich, and Patrick Keogh. Model-based condition monitoring of an auxiliary bearing following contact events. In *Proceedings of MOVIC 2010, August 17-20, 2010, Tokyo, Japan*, 2010.

[27] Christoph Glocker. *Set-valued force laws in rigid body dynamics : dynamics of non-smooth systems*, volume 1 of *Lecture notes in applied and computational mechanics*. Springer, Berlin, 1st edition edition, 2001. ISBN 978-3-540-41436-0.

[28] Ernst Hairer. Symmetric projection methods for differential equations on manifolds. *BIT*, 40:726–734, 2000. ISSN 0006-3835.

[29] Ernst Hairer and Gerhard Wanner. *Solving Ordinary Differential Equations I: Nonstiff Problems*, volume 8 of *Springer series in computational mathematics*. Springer, Berlin, 2nd rev. edition, 1st softcover printing edition, 2009. ISBN 978-3-642-05163-0.

[30] Ernst Hairer and Gerhard Wanner. *Solving Ordinary Differential Equations II: Stiff and Differential-Algebraic-Problems*, volume 14 of *Springer series in computational mathematics*. Springer, Berlin, 2nd rev. edition, 1st softcover printing edition, 2010. ISBN 978-3-642-05220-0.

[31] Hans Hilber, Thomas Hughes, and Robert Taylor. Improved numerical dissipation for time integration algorithms in structural dynamics. *Earthquake Eng Struct Dynam*, 5(3):283–292, 1977. ISSN 1096-9845.

[32] Robert Huber and Heinz Ulbrich. Higher order integration of non-smooth dynamical systems using parallel computed extrapolation methods based on time-stepping schemes. In *Proceedings of 1st*

Joint International Conference on Multibody System Dynamics, Lappeenranta, 25th-27th May 2010, 2010. ISBN 978-952-214-778-3.

[33] Michel Jean. The nonsmooth contact dynamics method. *Comput Methods Appl Mech Engrg*, 177: 235–257, 1999. ISSN 0045-7825.

[34] Kenneth Johnson. *Contact Mechanics*. Cambridge University Press, New York, 2008. ISBN 978-0521347969.

[35] Danny Kaufman and Dinesh Pai. Geometric numerical integration of inequality constrained, nonsmooth Hamiltonian systems. *SIAM J Sci Comput*, 34:2670–2703, 2012. ISSN 1064-8275.

[36] Rolf Krause and Mirjam Walloth. Presentation and comparison of selected algorithms for dynamic contact based on the newmark scheme. *Appl Numer Math*, 62(10):1393 – 1410, 2012. ISSN 0168-9274.

[37] Tod Laursen. *Computational contact and impact mechanics*. Springer, 2002. ISBN 3-540-42906-9.

[38] Remco Ingmar Leine and Nathan van de Wouw. *Stability and convergence of mechanical systems with unilateral constraints*, volume 36 of *Lecture notes in applied and computational mechanics*. Springer, Berlin, 2008. ISBN 978-3-540-76975-0.

[39] Christian Lubich. Extrapolation integrators for constrained multibody systems. *Impact of Computing in Science and Engineering*, 3(3):213–234, 1991. ISSN 0899-8248.

[40] Jerrold Marsden and Matthew West. Discrete mechanics and variational integrators. *Acta Numerica*, 10:357–514, 2001. ISSN 0962-4929.

[mbsim] mbsim. MBSim - multi-body simulation software. GNU Lesser General Public License `http://code.google.com/p/mbsim-env/`.

[41] Robert McLachlan and Reinout Quispel. Splitting methods. *Acta Numerica*, 11:341–434, 1 2002. ISSN 1474-0508.

[42] Jean Jacques Moreau. Numerical aspects of the sweeping process. *Comput Methods Appl Mech Engrg*, 177:329–349, 1999. ISSN 0045-7825.

[43] Ander Murua. Phem 56 user's guide. Technical report, Universite de Geneve, Suisse, 1995.

[44] Ander Murua. Partitioned half-explicit runge-kutta methods for differential-algebraicsystems of index 2. *Computing*, 59(1):43–61, 1997. ISSN 0010-485X.

[45] Nathan Newmark. A method for computation for structural dynamics. *J Eng Mech*, 85(EM 3): 67–94, 1959. ISSN 0733-9399.

[46] Laetitia Paoli and Michelle Schatzman. A numerical scheme for impact problems i: the one-dimensional case. *SIAM J Numer Anal*, 40:702–733, 2002. ISSN 0036-1429.

[47] Laetitia Paoli and Michelle Schatzman. A numerical scheme for impact problems i: the multidimensional case. *SIAM J Numer Anal*, 40:734–768, 2002. ISSN 0036-1429.

[48] Friedrich Pfeiffer. *Mechanical system dynamics*, volume 40 of *Lecture notes in applied and computational mechanics*. Springer, Berlin, corr. 2nd printing edition, 2008. ISBN 978-3-540-79435-6.

[49] Liqun Qi and Defeng Sun. A survey of some nonsmooth equations and smoothing newton methods. In *Progress in Optimization*, volume 30 of *Applied Optimization*, pages 121–146. Springer US, 1999. ISBN 978-1-4613-3287-9.

[50] Ralph Tyrrell Rockafellar. *Convex Analysis*. Princeton University Press, Princeton, 10th printing and 1st paperb. printing edition, 1997. ISBN 0-691-01586-4.

[51] Thorsten Schindler and Vincent Acary. Timestepping schemes for nonsmooth dynamics based on discontinuous Galerkin methods: definition and outlook. *Math Comput Simulat*, 95:180–199, 2013. ISSN 0378-4754.

[52] Thorsten Schindler, Martin Förg, Markus Friedrich, Markus Schneider, Bastian Esefeld, Robert Huber, Roland Zander, and Heinz Ulbrich. Analysing dynamical phenomenons: introduction to MBSim. In *Proceedings of 1st Joint International Conference on Multibody System Dynamics, Lappeenranta, 25th-27th May 2010*, 2010. ISBN 978-952-214-778-3.

[53] Thorsten Schindler, Binh Nguyen, and Jeff Trinkle. Understanding the difference between prox and complementarity formulations for simulation of systems with contact. In *IEEE/RSJ International Conference on Intelligent Robots and Systems, San Francisco, 25th-30th September 2011*, 2011. ISBN 978-1-61284-454-1.

[54] Svenja Schoeder, Heinz Ulbrich, and Thorsten Schindler. Discussion of the Gear-Gupta-Leimkuhler method for impacting mechanical systems. *Multibody System Dynamics*, 31:477–495, 2014. ISSN 1384-5640.

[55] Bernd Simeon. *Computational Flexible Multibody Dynamics*. Springer, Berlin, 2013. ISBN 978-3-642-35157-0.

[56] Juan Simo and Nils Tarnow. The discrete energy-momentum method. conserving algorithms for nonlinear elastodynamics. *Z Angew Math Phys*, 43(5):757–792, 1992. ISSN 0044-2275.

[57] David Stewart. Rigid-body dynamics with friction and impact. *SIAM Rev*, 42:3–39, 2000. ISSN 1095-7200.

[58] David Stewart. *Dynamics with inequalities*. SIAM, Philadephia, 2011. ISBN 978-1-611-97071-5.

[59] Christian Studer. *Numerics of unilateral contacts and friction : modeling and numerical time integration in non-smooth dynamics*, volume 47 of *Lecture notes in applied and computational mechanics*. Springer, Berlin, 2009. ISBN 978-3-642-01099-6.

[60] Barbara Wohlmuth. Variationally consistent discretization schemes and numerical algorithms for contact problems. *Acta Numerica*, 20:569–734, 5 2011. ISSN 1474-0508.

[61] Peter Wriggers. *Computational contact mechanics*. Wiley, Chichester, 1st edition edition, 2002. ISBN 0-471-49680-4.

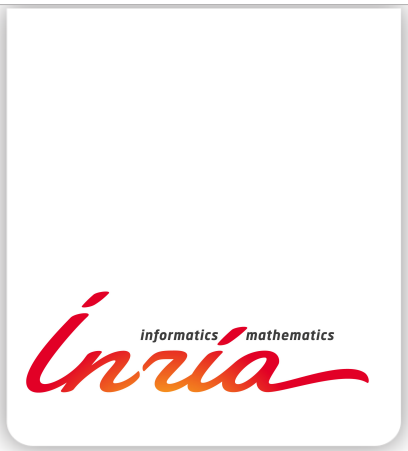

RESEARCH CENTRE
GRENOBLE – RHÔNE-ALPES

Inovallée
655 avenue de l'Europe Montbonnot
38334 Saint Ismier Cedex

Publisher
Inria
Domaine de Voluceau - Rocquencourt
BP 105 - 78153 Le Chesnay Cedex
inria.fr

ISSN 0249-6399